Supplemental Note 1. Role of transcription factors in recruitment of KDM1A to enhancers

Higher KDM1A occupancy at more active enhancers may contradict with the KDM1A's role as a transcriptional repressor of neuron-specific genes in non-neuronal tissues (Hakimi et al. 2002; Shi et al. 2004). We sought to test if KDM1A is involved in silencing of lineage-specific transcriptional enhancers in mESCs. Cell type-specific enhancers can be inert, i.e., free of TFs, and therefore, insensitive to DNase I in other cell types and KDM1A may bind to such TF-free enhancers. We first looked at the *mir290* cluster, which is transcriptionally active in mESCs and early developmental stages (Jouneau et al. 2012). In mESCs, several enhancers upstream of its promoter show high DHS, high EP300 binding, and high GRO-seq signals accompanied by strong KDM1A binding (Supplemental Fig. S6A). These *mir290* enhancers lacked any brain-derived DHS, GRO-seq signals, and H3K4 methylation in cortical neurons (CN), demonstrating that these enhancers are primed in mESCs but are inert in cortical neurons (Supplemental Fig. S6A). KDM1A ChIP-seq data from neural stem cells (NSC) (Wang et al. 2016) showed a lack of KDM1A binding at the *mir290* enhancers in NSC (Supplemental Fig. S6A). Conversely, two enhancers upstream of *Npas4* (marked with asterisks, Supplemental Fig. S6B), a gene predominantly expressed in the brain, showed brain-specific DHS, KDM1A occupancy, GRO-seq signals, and high H3K4me1, specifically in NSC or cortical neurons. In mESCs, KDM1A is absent at these brain-specific DHS sites upstream of the *Npas4* promoter (Supplemental Fig. S6B). These two examples suggest that KDM1A may be recruited to enhancers in a TF-dependent manner.

To ascertain this specificity of KDM1A recruitment to TF-bound enhancers on a genome-wide scale, we sought to identify genomic elements that are DNase I-insensitive in mESCs but are DNase I-sensitive in other cell types. To this end, we analyzed publicly available DNase I Digital Genomic Footprinting (DGF) data (Neph et al. 2012) and identified DHS sites from mESCs (398,675, $q < 0.01$) and four additional mouse tissues, including the adult brain (415,400), heart (320,416), liver (207,046), and lung (358,575), using Hotspot (v4.1) (John et al. 2011). Similar to our earlier observation (Supplemental Fig. S1), we found that most of the mESC KDM1A peaks (86%) overlapped with mESC hotspots (Supplemental Fig. S6C). Next, we performed an intersection of hotspots from the five tissues. The intersection resulted in tens of thousands of hotspots, which could potentially act as tissue-specific enhancers in a given tissue and are inert in others. Motif analysis on promoter-distal hotspots revealed that these tissue-specific hotspots are indeed enriched with binding sites for lineage-specific TFs (Supplemental Fig. S7). In agreement with the *mir290* and *Npas4* loci, mESC KDM1A binding sites showed negligible overlaps with the tissue-specific hotspots (0.40-0.69%), whereas 14.31% of mESC-specific hotspots were bound by KDM1A in mESCs (Supplemental Fig. S6D and S6E). These observations suggest that KDM1A is predominantly recruited to TF-bound enhancers and is not actively involved in silencing of lineage-specific enhancers in mES cells.

To examine which TFs can potentially recruit KDM1A to mESC enhancers, we performed a motif analysis on KDM1A-bound enhancers using FIMO (Grant et al. 2011). We found that 9,562 (68.6%) of the 13,937 KDM1A-bound enhancers showed an enrichment of the motifs of the three pluripotency TFs: SOX2, POU5F1, and NANOG (Supplemental Table S3). Inclusion of CTCF, ESR1, ESR2, and NR5A2 could cumulatively account for almost all (13,851, 99.4%) of the KDM1A-bound enhancers in mESCs.

FODXD3 interacts with and recruits KDM1A to mESC enhancers (Respuela et al. 2016). Our motif search showed that 4,516 (32.04%) of KDM1A-bound enhancers showed an enrichment of either the reported FOXD3 motif or the highly-related FOXD1 motifs from HOCOMOCO (Kulakovskiy et al. 2018). However, in contrast to the pluripotency TFs, the motif enrichment was not statistically significant. We also analyzed FOXD3 ChIP-seq dataset (Respuela et al. 2016) and found that 2,225 (15.96%) of KDM1A-bound enhancers were positive for FOXD3 binding suggesting that a subset of enhancers could be cooperatively regulated by KDM1A and FOXD3. However, our analysis indicates that in mESCs, KDM1A is predominantly recruited to the enhancers by the pluripotency TFs, such as SOX2, POU5F1, NANOG, and KLF4.

Supplemental Note 2. Effect of loss of KDM5C on activity of enhancers in mESCs

We identified 11,483 out of a total of 22,047 enhancers to be co-occupied by KDM1A and KDM5C (Fig. 3A) in mESCs. Upon the loss of KDM1A in mESCs, 3,011 of these enhancers were upregulated and 543 were downregulated ($q < 0.05$, DESeq). Using the same significance cutoff, we were unable to identify any misregulated enhancers in *Kdm5c*-KO mESCs. After relaxing the cutoff to $p < 0.05$, we could identify only 41 upregulated and 75 downregulated enhancers in *Kdm5c*-KO mESCs (Fig. 3D). We confirmed that these observations were not dependent on differences in sequencing depths or inter-replicate variability, by randomly selecting same number of reads from each GRO-seq sample and repeating the pairwise comparisons between individual replicates of different genotypes. These results highlight that, in contrast to KDM5C, KDM1A plays an essential role in regulation of enhancers in mESCs.

KDM5C has been shown to either promote enhancer activity by generating H3K4me1 in mESCs (Outchkourov et al. 2013) or prevent overactivation of enhancers in breast cancer cells (Shen et al. 2016). However, we did not observe a global change in eRNA levels upon the loss of KDM5C in mESCs. *Kdm5a* and *Kdm5b* are expressed in mESCs at levels similar to those of *Kdm5c* and could possibly compensate for the loss of KDM5C in mESCs. Alternatively, the requirement of KDM5C could be restricted to only a small set of enhancers in mESCs and was not explored further in this study.

Supplemental Note 3. Roles of KDM1A and its catalytic activity in regulation of enhancers

The cDNA complementation study in the inducible *Kdm1a*-KO mESCs showed that similarly to the re-expression of WT KDM1A, the catalytic hypomorphic mutant KDM1A-K661A could downregulate most of the eRNAs tested. The observation suggests that KDM1A-mediated suppression of enhancer activity also involves demethylase activity-independent mechanisms (Fig. 3F). The results were consistent with the previous observation in human ES cells that KDM1A can suppress gene expression in both enzymatic activity-dependent and -independent manners (Adamo et al. 2011). The non-enzymatic functions of KDM1A may involve the assembly of stable repressive complexes at promoters and enhancers. For example, loss of KDM1A results in the protein instability of CoREST (Foster et al. 2010; Macfarlan et al. 2011) and KDM1A exerts its repressive activity through physical interactions with various cofactors, such as GFI1 (Maiques-Diaz et al. 2018). Given the increased H3K27ac and unchanged HDAC1 at enhancers in KDM1A-deficient mESCs (Fig. 2), a plausible scenario is an allosteric augmentation of the deacetylase activity of HDAC1 by KDM1A. The recently observed interdependency between the deacetylase and the demethylase activities within the KDM1A-CoREST-HDAC1 complex supports this possibility (Song et al. 2020).

Supplemental Note 4. Contribution of the KDM1A neuronal isoform in regulation of activity-regulated genes and enhancers

KDM1A has a neuron-specific isoform, neuroLSD1 or LSD1n, with four extra amino acids in its catalytic domain (Zibetti et al. 2010). The substrate specificity of the neuronal isoform remains ambiguous (Laurent et al. 2015; Wang et al. 2015). Since our RNAi approach in cortical neurons depleted both the canonical and the neuronal isoforms of KDM1A, it remains unclear whether the loss of one or both of the isoforms mediated the spurious activation of activity-regulated enhancers and ARGs. Given that the genetic ablation of neuroLSD1 resulted in a downregulation of ARGs (Wang et al. 2015; Rusconi et al. 2016), the canonical KDM1A, not the neuronal isoform, seems more likely to be responsible for the suppression of activity-regulated enhancers in this study.

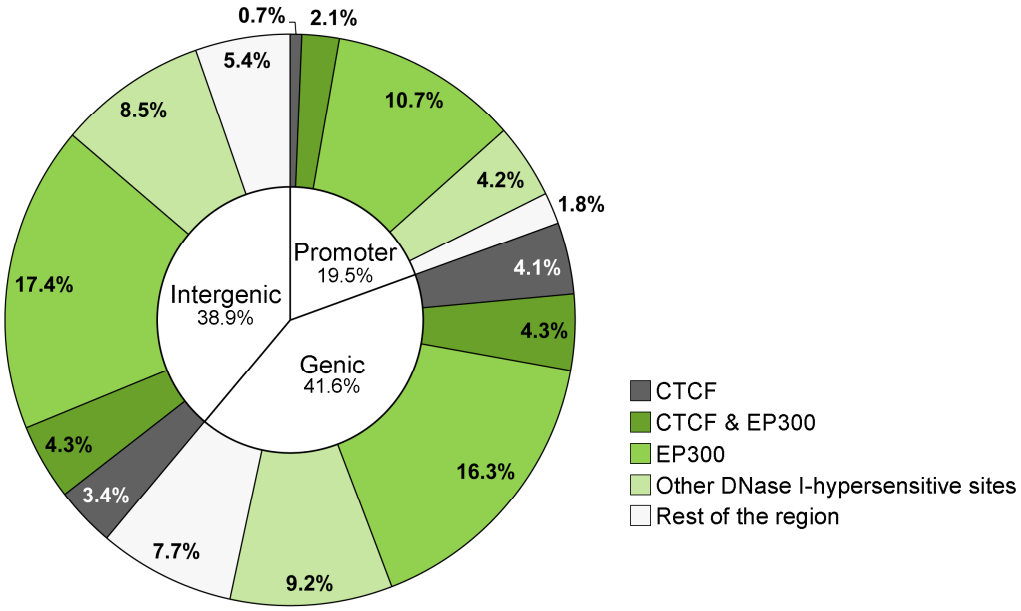

Supplemental Figure S1. Overlap of KDM1A binding sites with EP300, CTCF, and DHS sites across the genome. Promoter regions were defined as ± 1 kb of transcription start sites (TSSs). Genic regions were defined as 1 kb downstream of TSSs to 1 kb downstream of transcription termination sites, and the rest of the genome was defined as intergenic regions. KDM1A shows a small overlap (8.11%) with CTCF-only sites, which represent insulator regions. In contrast, KDM1A occupies a large fraction of EP300 and DHS sites, which represent other regulatory elements such as enhancers. KDM1A, CTCF, EP300, and DHS peaks were extended to ± 250 bases of the peak summits for the intersection analysis.

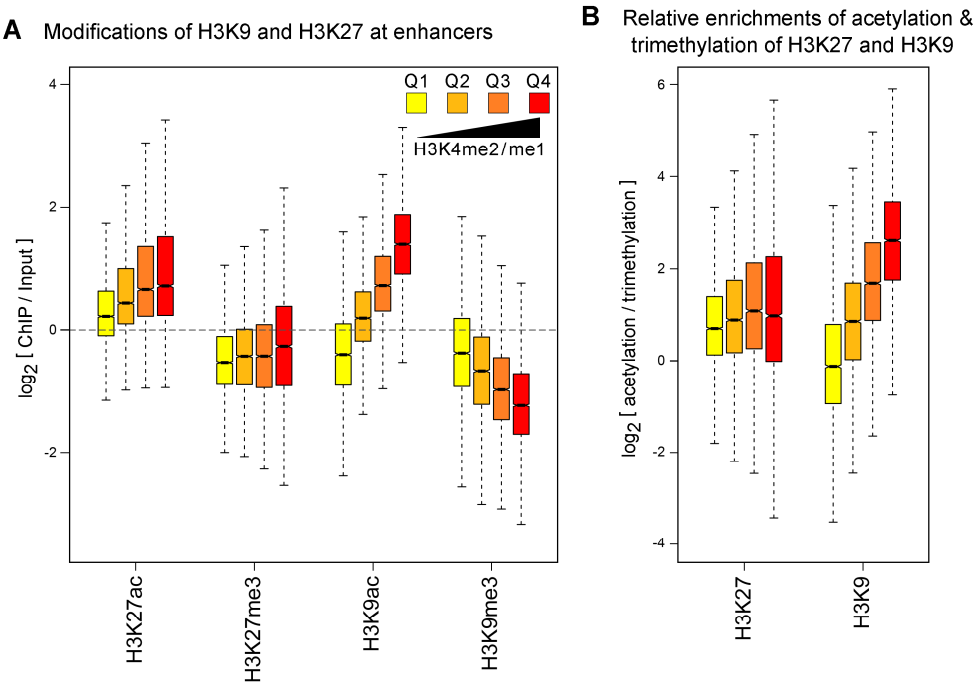

Supplemental Figure S2. Relationships between levels of H3K4 methylations and levels of acetylation and methylation at H3K9 and H3K27 at enhancers. (**A**) Acetylation (ac) and tri-methylation (me3) of H3K9 and H3K27 are plotted for each quartile (Q1-Q4) of intergenic enhancers divided according to the relative enrichment of H3K4me2 to H3K4me1. While H3K27ac and H3K9ac correlate strongly with the H3K4me2/me1 ratio, H3K27me3 and H3K9me3 show either a weak positive correlation a strong negative correlation with the H3K4me2/me1 ratio at the enhancers, respectively. (**B**) The acetylation: trimethylation ratios of H3K27 and H3K9 increase from Q1 to Q4 with an increase in the H3K4me2/me1 ratio at enhancers.

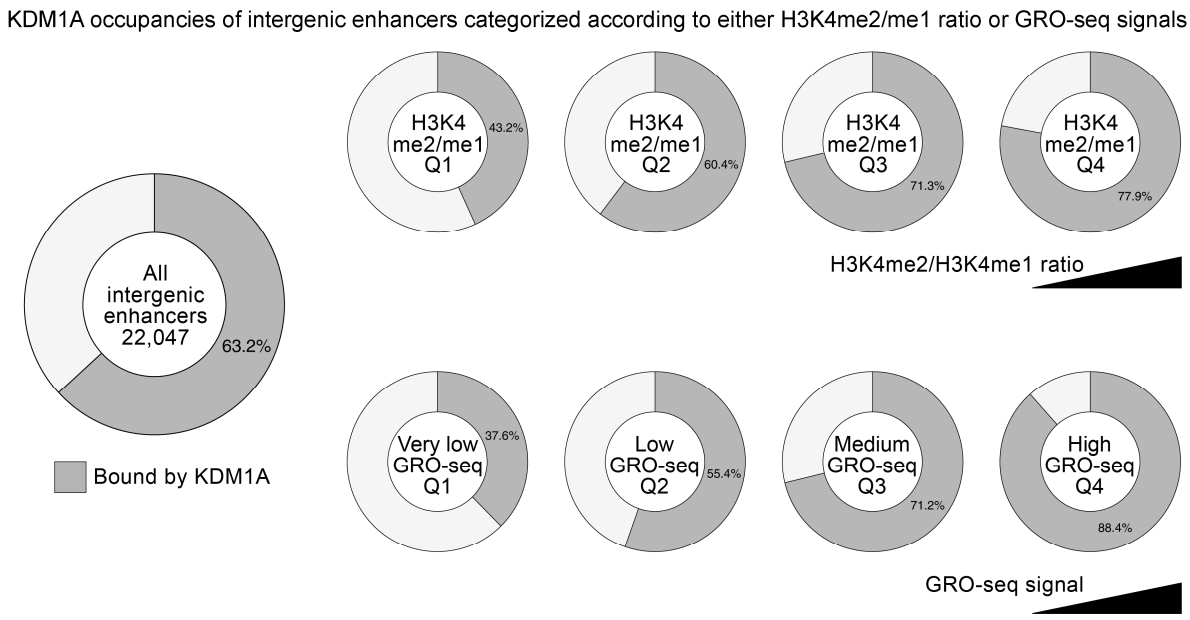

Supplemental Figure S3. KDM1A shows increased occupancies at enhancers with increasingly higher H3K4me2 or increasingly higher enhancer activity. Fractions of KDM1A-bound and -unbound enhancers in each quartile of intergenic enhancers categorized according to either H3K4me2/me1 ratio or eRNA transcription levels. Enhancers were defined as ±500 bases of EP300 or DHS summits.

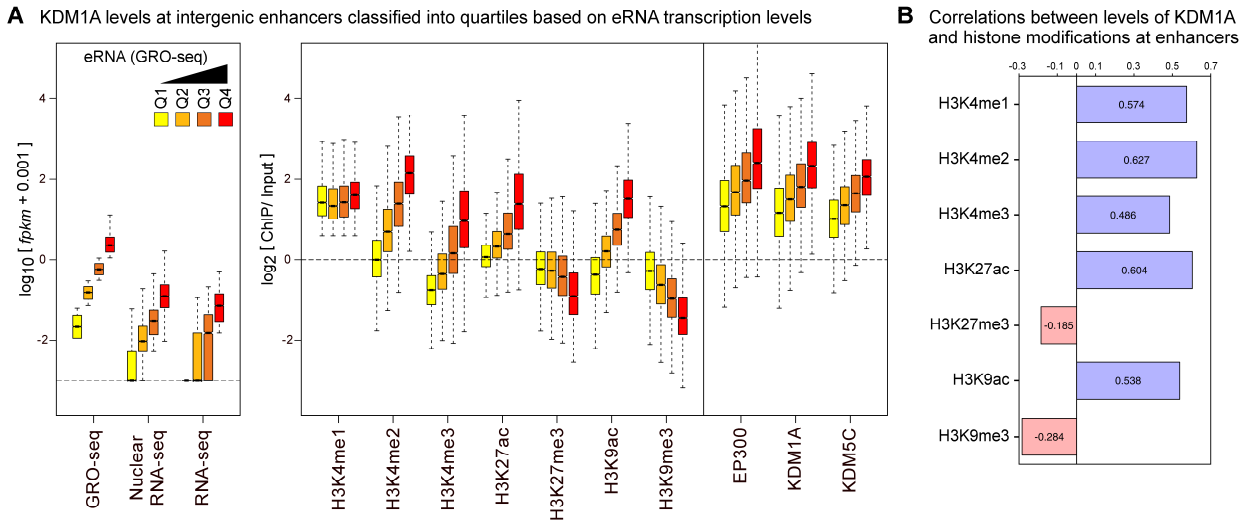

Supplemental Figure S4. KDM1A levels at intergenic enhancers correlate positively with enhancer activity. (**A**) Enhancer classification based on eRNA levels. The intergenic enhancers were classified into quartiles based on GRO-seq signals (Q1-Q4, left panel). Levels of indicated histone modifications, EP300, KDM1A, and KDM5C are plotted for the Q1-Q4 set of enhancers (right panel). KDM1A levels correlate positively with eRNA transcription levels and H3K4me2. In contrast to other histone modifications, H3K9me3 and H3K27me3 show inverse correlations with eRNA and KDM1A levels. (**B**) Correlation coefficients between enrichment of KDM1A and indicated histone modifications at 167,773 promoter-distal EP300/DHS sites (excluding TSS ± 1.5 kb). KDM1A levels show the strongest positive correlations with H3K4me2 and H3K27ac and negative correlations with H3K9me3 and H3K27ac. Correlation coefficients were calculated after $\log_2$ transformation of ChIP: Input ratio for KDM1A and various histone modifications.

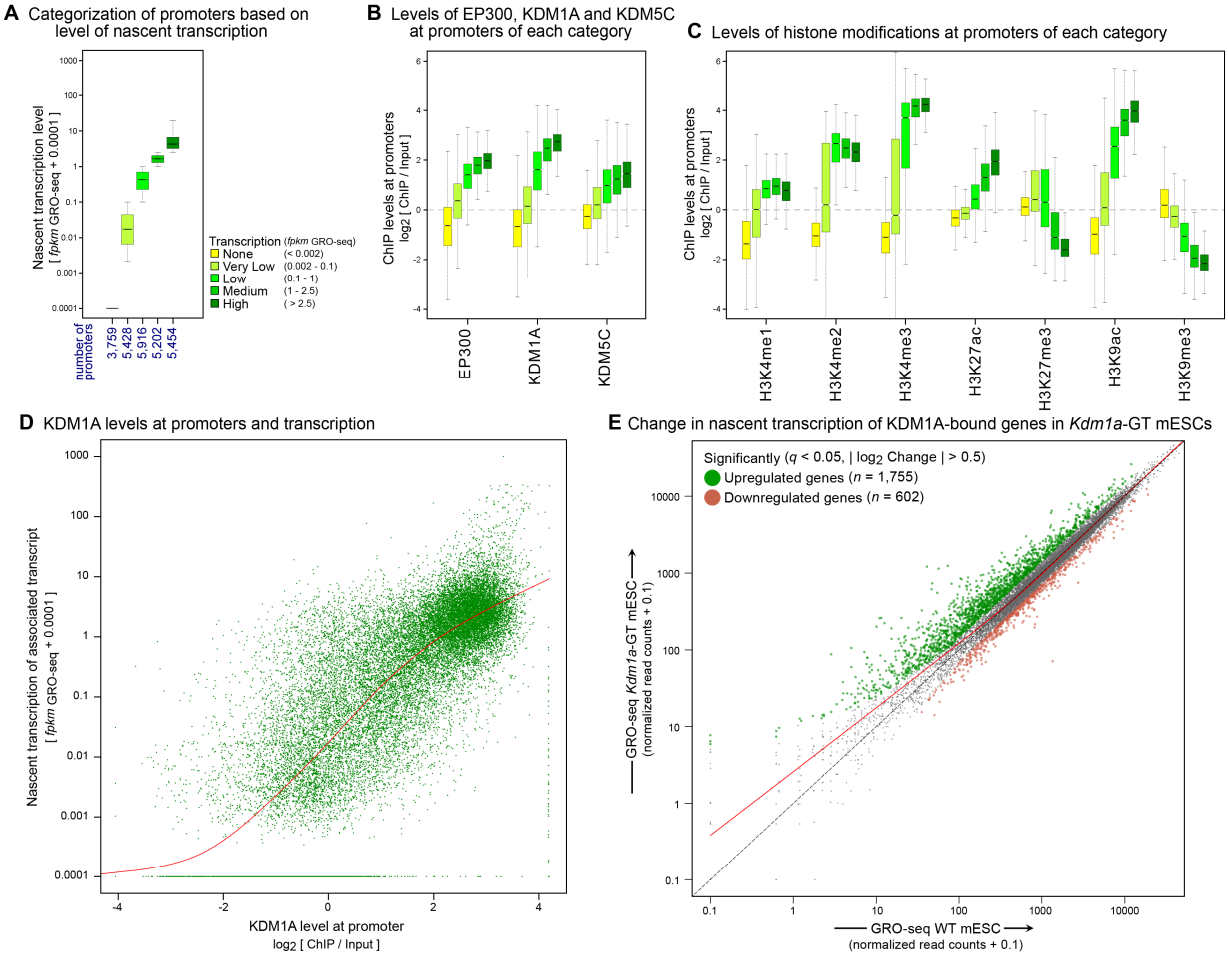

Supplemental Figure S5. Relationships between the levels of KDM1A and histone modifications at promoters and nascent transcription. (**A**) Categorization of promoters into approximate quintiles based on GRO-seq *fpkms* of the genes. (**B**) ChIP-seq signals of EP300, KDM1A, and KDM5C, normalized to input, at promoters of each quintile. (**C**) Levels of histone modifications at promoters of each quintile. (**D**) Scatter plot representing the relationship between KDM1A levels at promoters and nascent transcription of genes. (**E**) Changes in nascent transcription of genes that are bound by KDM1A at their promoters upon the loss of KDM1A in mESCs. Red lines: LOWESS fitting curves.

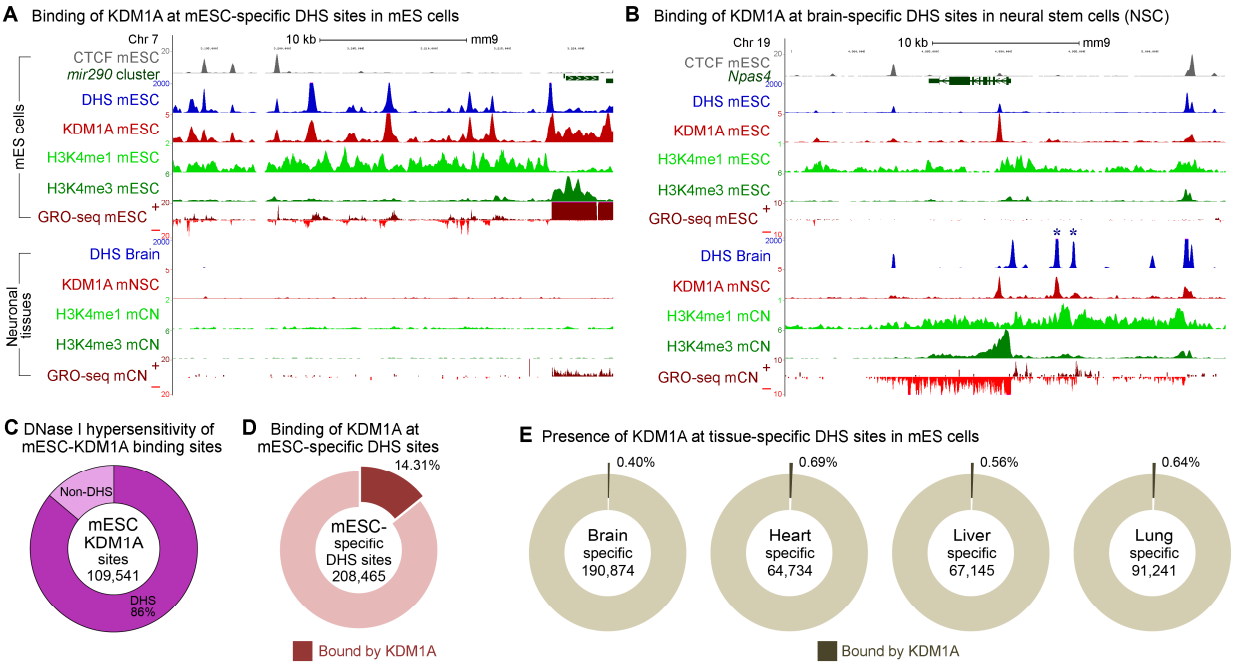

Supplemental Figure S6. KDM1A rarely binds to lineage-specific enhancers that are DNase I insensitive in a given cell type. (**A**) UCSC genome browser snapshot of the *mir290* locus. KDM1A ChIP-seq peaks in mESCs coincide with enhancer signatures, including DHS, H3K4me1, and divergent GRO-seq signals, upstream of the *mir290* promoter in mESCs but not in neuronal cells. (**B**) KDM1A binding at the *Npas4* locus in mESCs and NSC. KDM1A is present at the two brain-specific DHS sites (marked by asterisks) in neuronal cells but not in mESCs. Note that the DHS sites common in the adult brain and mESCs are occupied by KDM1A in both mESCs and NSC. NSC: Neural stem cells, CN: Cortical neurons. CTCF, DHS, and KDM1A tracks were generated from previously published datasets. (**C**) Fraction of KDM1A peaks in mESCs overlapping with mESC hotspots. (**D**) Fraction of mESC-specific hotspots overlapping with mESC KDM1A peaks. (**E**) Fractions of tissue-specific hotspots overlapping with KDM1A peaks in mESCs.

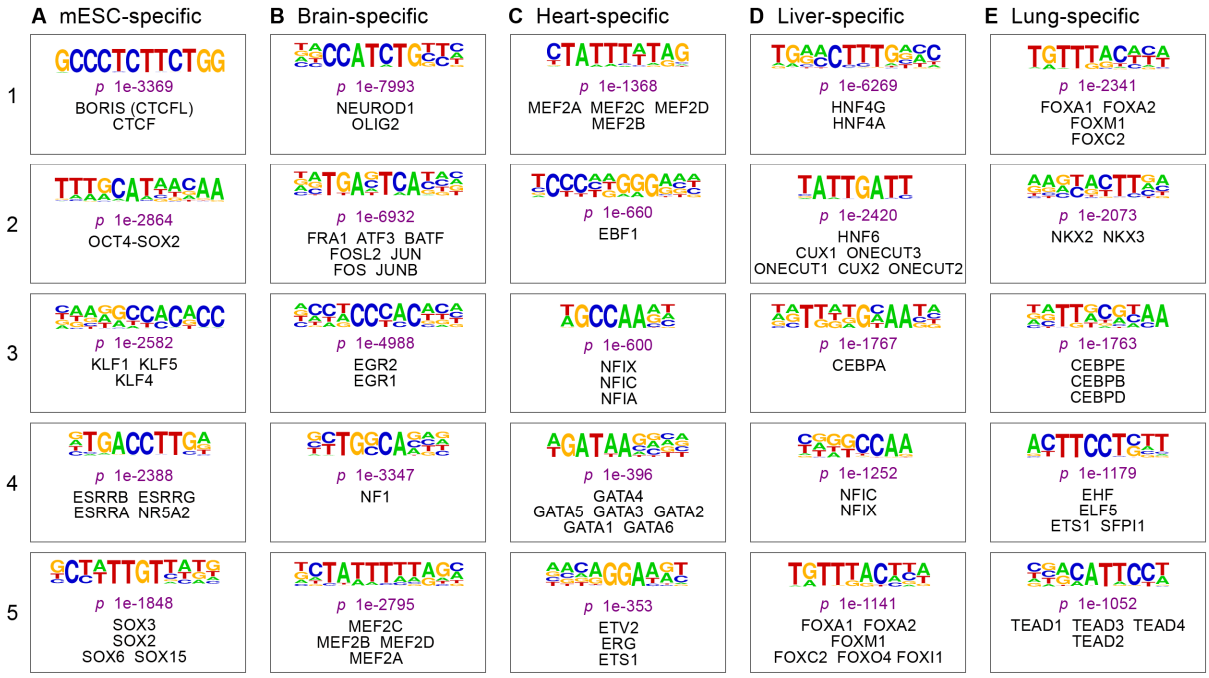

Supplemental Figure S7. Promoter distal tissue-specific hotspots are enriched for lineage-specific TF-binding sites. Results from HOMER motif analysis (Heinz et al. 2010) of the tissue-specific hotspots (John et al. 2011) derived from mESCs (**A**), brain (**B**), heart (**C**), liver (**D**), and lung (**E**) DNase I Digital Genomic Footprinting (DGF) data (Neph et al. 2012). Promoter regions were defined as ±2 kb of known TSSs.The five most significantly enriched motifs from each tissue are shown. *P*-values of enrichment of motifs are shown in purple.

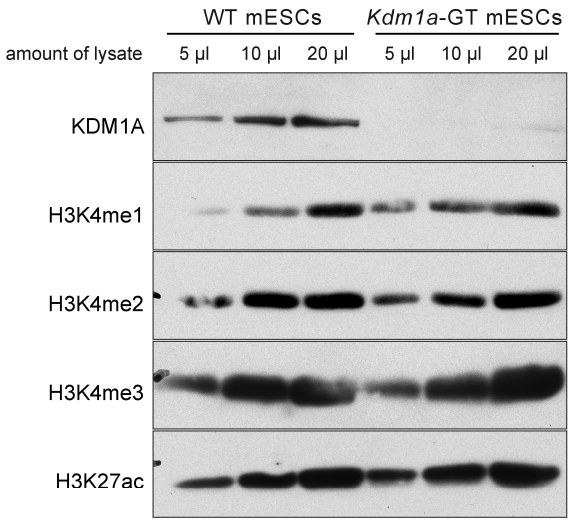

Supplemental Figure S8. Loss of KDM1A in *Kdm1a*-GT mESCs does not result in a significant change in global levels of H3K4 methylations or H3K27ac. Western blot analysis of whole-cell extracts to compare the global levels of indicated histone modifications in WT and *Kdm1a*-GT mESCs. While the loss of KDM1A in *Kdm1a*-GT mESCs was confirmed, no noticeable differences were observed in global levels of H3K4me1, H3K4me2, H3K4me3, or H3K27ac.

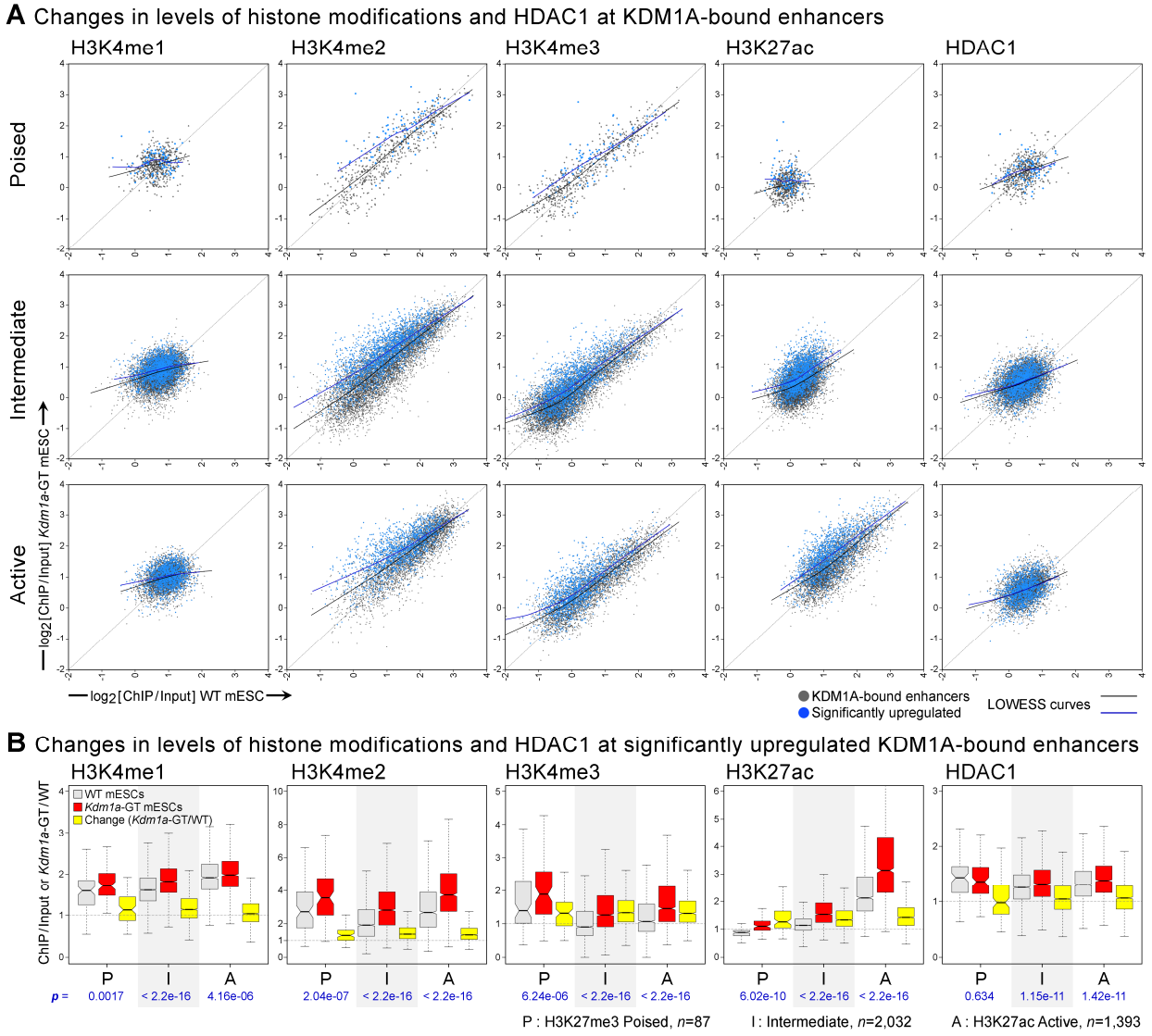

Supplemental Figure S9. Loss of KDM1A results in increased H3K4 methylations and H3K27ac at poised, intermediate, and active enhancers. (**A**) Levels of histone modifications and HDAC1 at KDM1A-bound intergenic enhancers in WT and *Kdm1a*-GT mESCs. ChIP enrichment over the input (gray: KDM1A-bound enhancers, blue: significantly-upregulated enhancers) are plotted for *Kdm1a*-GT (Y-axis) and WT- (X-axis) mESCs. LOWESS curves represent fitting of all KDM1A-bound enhancers (black) and significantly-upregulated enhancers (blue). Significantly-upregulated enhancers are associated with marked increases in H3K4me2, H3K4me3, and H3K27ac as indicated by the differences in the two fitting curves. The shapes of the LOWESS curves underscore the observation that while many enhancers gain these modifications upon the loss of KDM1A, enhancers harboring higher levels of these chromatin modifications in WT mESCs tend to lose these marks in *Kdm1a*-GT mESCs. (**B**) Levels of indicated histone modifications and HDAC1 at KDM1A-bound intergenic enhancers that show significant upregulation of GRO-seq signals upon the loss of KDM1A in mESCs. ChIP enrichment over the input (gray: WT, red: GT) as well as the GT/WT ratio (yellow box) are plotted for poised (P), intermediate (I), and active (A) enhancers. *n* indicates the number of enhancers in each category. *P*-values (*p*) from Wilcoxon signed-rank tests of change, $\log_2$ (GT/WT), are indicated in blue.

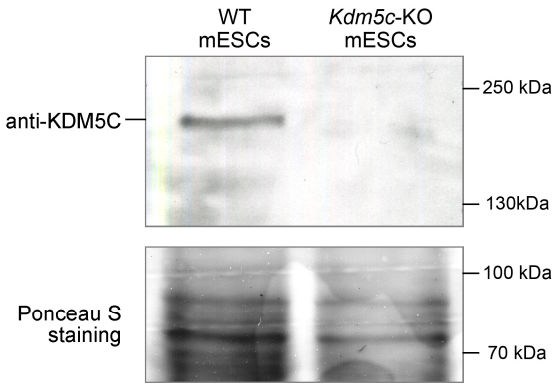

Supplemental Figure S10. Validation of the loss of KDM5C protein in *Kdm5c*-knockout (KO) mESCs. Western blot analysis to confirm the loss of KDM5C protein in *Kdm5c*-KO mESCs. Upper panel: anti-KDM5C antibody (Iwase et al. 2016), Lower panel: Ponceau S staining.

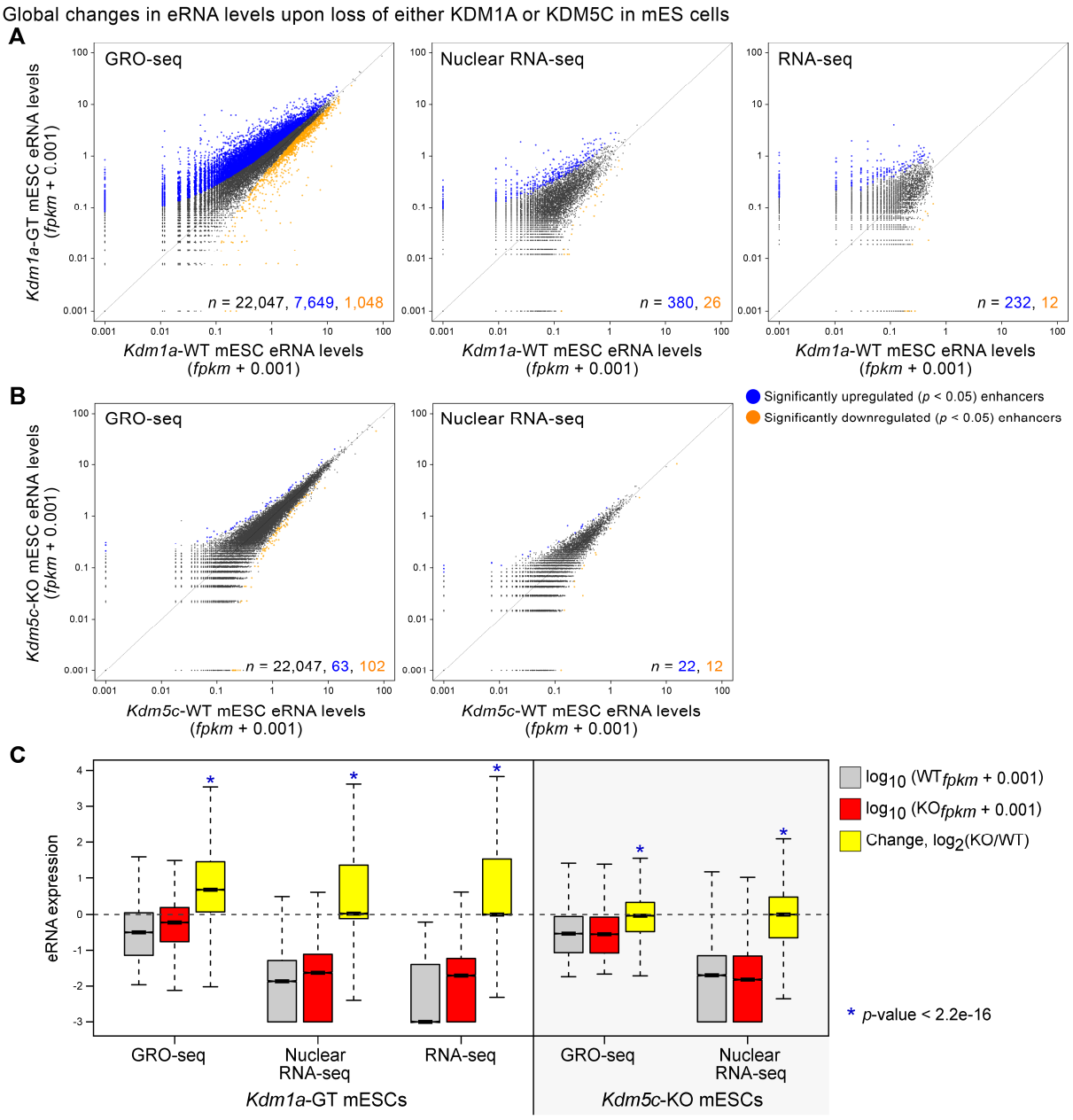

Supplemental Figure S11. Changes in eRNA levels upon the loss of either KDM1A or KDM5C in mESCs. Scatter plots of eRNA levels measured by GRO-seq, nuclear RNA-seq, and/or RNA-seq at all of the 22,047 intergenic enhancers in WT- and *Kdm1a*- GT(**A**) or *Kdm5c*-KO (**B**) mESCs. Significantly misregulated enhancers ($p < 0.05$, DESeq) are shown in blue (upregulated) and orange (downregulated). *n* indicates the number of significantly-upregulated and -downregulated enhancers. (**C**) Boxplots show global eRNA levels and changes at all intergenic enhancers. Gray boxes indicate WT mESCs, while red boxes indicate either the *Kdm1a*- (left panel) or *Kdm5c*- mutant (right panel) mESCs. Yellow boxes indicate $\log_2$ (eRNA change) in the mutant mESCs. eRNA levels measured by the three techniques show statistically-significant upregulation of eRNAs ($p < 2.2^{-16}$, Wilcoxon signed-rank test) in *Kdm1a*-GT mESCs. Loss of KDM5C results in a small but statistically-significant decrease in eRNA levels.

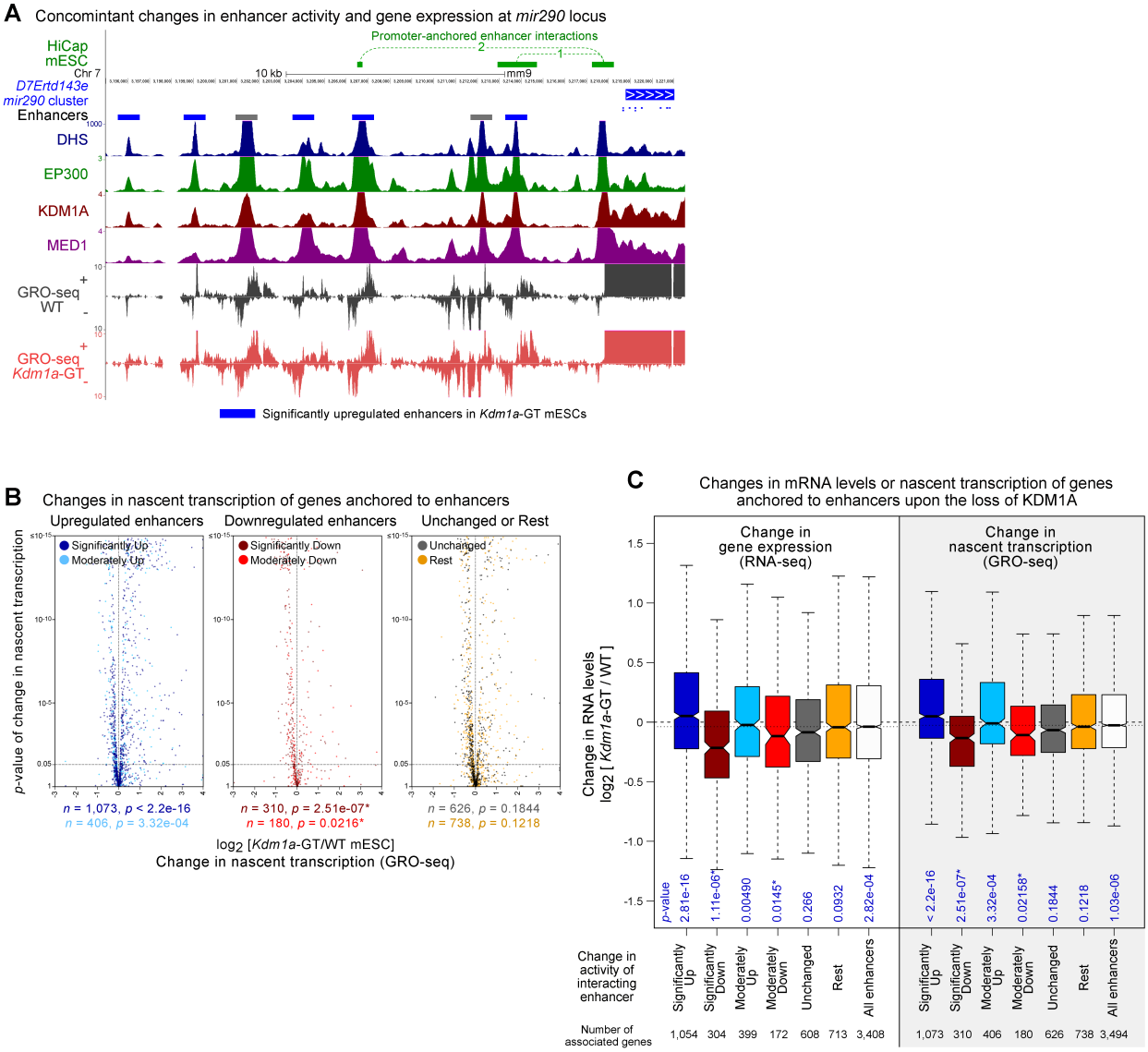

Supplemental Figure S12. Misregulation of enhancers and corresponding genes in *Kdm1a*-GT mESCs. (**A**) UCSC genome browser snapshot showing the misregulation of enhancers at the *mir290* locus, an ES-specific microRNA gene. Top track: Long-range interactions between enhancers and the *mir290* promoter in mESCs (HiCap (Sahlen et al. 2015)). Bars beneath the gene track represent predicted mESC enhancers (gray: all enhancers and blue: significantly upregulated enhancers). (**B**) Changes in nascent transcription of genes that physically interact with misregulated enhancers. Based on changes in eRNA transcription levels upon the loss of KDM1A, enhancers were subdivided as significantly up ($q < 0.05$, DESeq), significantly down, moderately up ($0.05 \leq q < 0.25$), moderately down, unchanged ($q \geq 0.5$ and fold change ≤ 25%) and the rest. Assignment of physically-interacting genes to each enhancer subgroup was prioritized according to the significance of changes in enhancer activity. Volcano plots display the changes in GRO-seq signals of the gene groups in *Kdm1a*-GT mESCs compared to WT mESCs. Note that more genes anchored to upregulated enhancers are upregulated compared to genes that interact with downregulated enhancers. (**C**) Boxplots of changes in either expression (left panel, RNA-Seq) or nascent transcription (right panel, GRO-seq) of genes interacting with misregulated enhancers. *Kdm1a*-GT/WT ratios of RNA levels (left) and GRO-seq signals (right) of these gene groups are plotted. Blue boxes: Upregulated. Red boxes: Downregulated. Gray boxes: Unchanged. Orange boxes: Rest. The total number of genes (*n*) in each gene category and *p*-values (*p*) from Wilcoxon signed-rank tests on differences between the genotypes are shown beneath each panel. Genes with no read coverage in both WT mESCs and *Kdm1a*-GT mESCs were excluded.

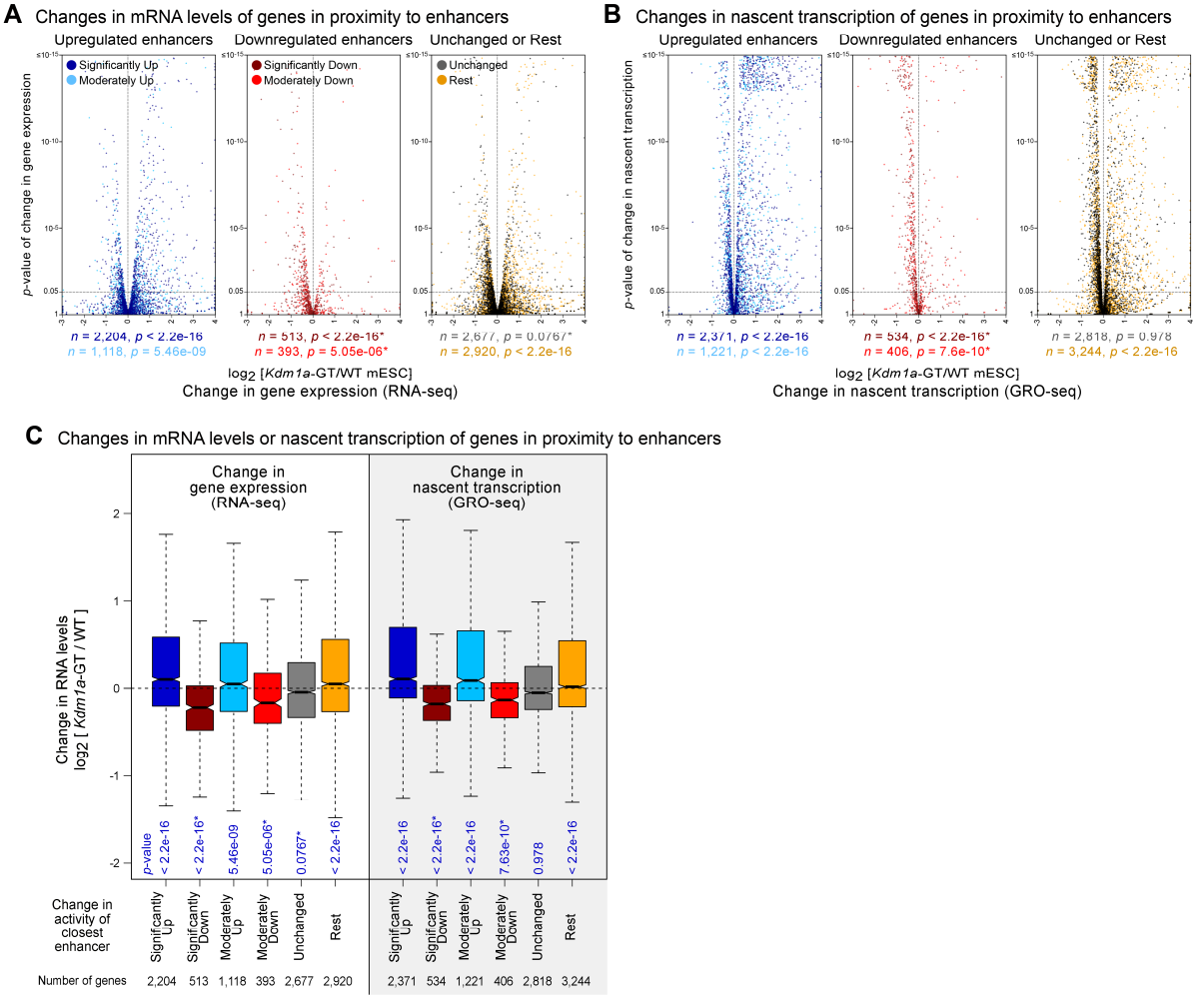

Supplemental Figure S13. Misregulation of genes in proximity to misregulated enhancers in *Kdm1a*-GT mESCs. Volcano plots of changes in expression (RNA-seq) (**A**) and nascent transcription (GRO-seq) (**B**) of genes that are in proximity to misregulated enhancers. Based on changes in eRNA transcription levels upon the loss of KDM1A, enhancers were subdivided as significantly up ($q < 0.05$, DESeq), significantly down, moderately up ($0.05 \leq q < 0.25$), moderately down, unchanged ($q \geq 0.5$ and fold change ≤ 25%) and the rest. Closest enhancers were assigned to a gene if they were located within 50 kb on either side of the gene promoter. The assignment of genes to each enhancer subgroup was prioritized in the aforementioned order. Note that genes in proximity to upregulated enhancers are upregulated compared to genes that are close to downregulated enhancers. (**C**) Boxplots of changes in either expression (left panel, RNA-seq) or nascent transcription (right panel, GRO-seq) of genes in proximity to misregulated enhancers. *Kdm1a*-GT/WT ratios of mRNA levels (left) and GRO-seq signals (right) of these gene groups are plotted. Blue boxes: Upregulated. Red boxes: Downregulated. Gray boxes: Unchanged. Orange boxes: Rest. The total number of genes (*n*) in each gene category and *p*-values (*p*) from Wilcoxon signed-rank tests on differences between the genotypes are shown beneath each panel. Genes with no read coverage in both WT mESCs and *Kdm1a*-GT mESCs were excluded.

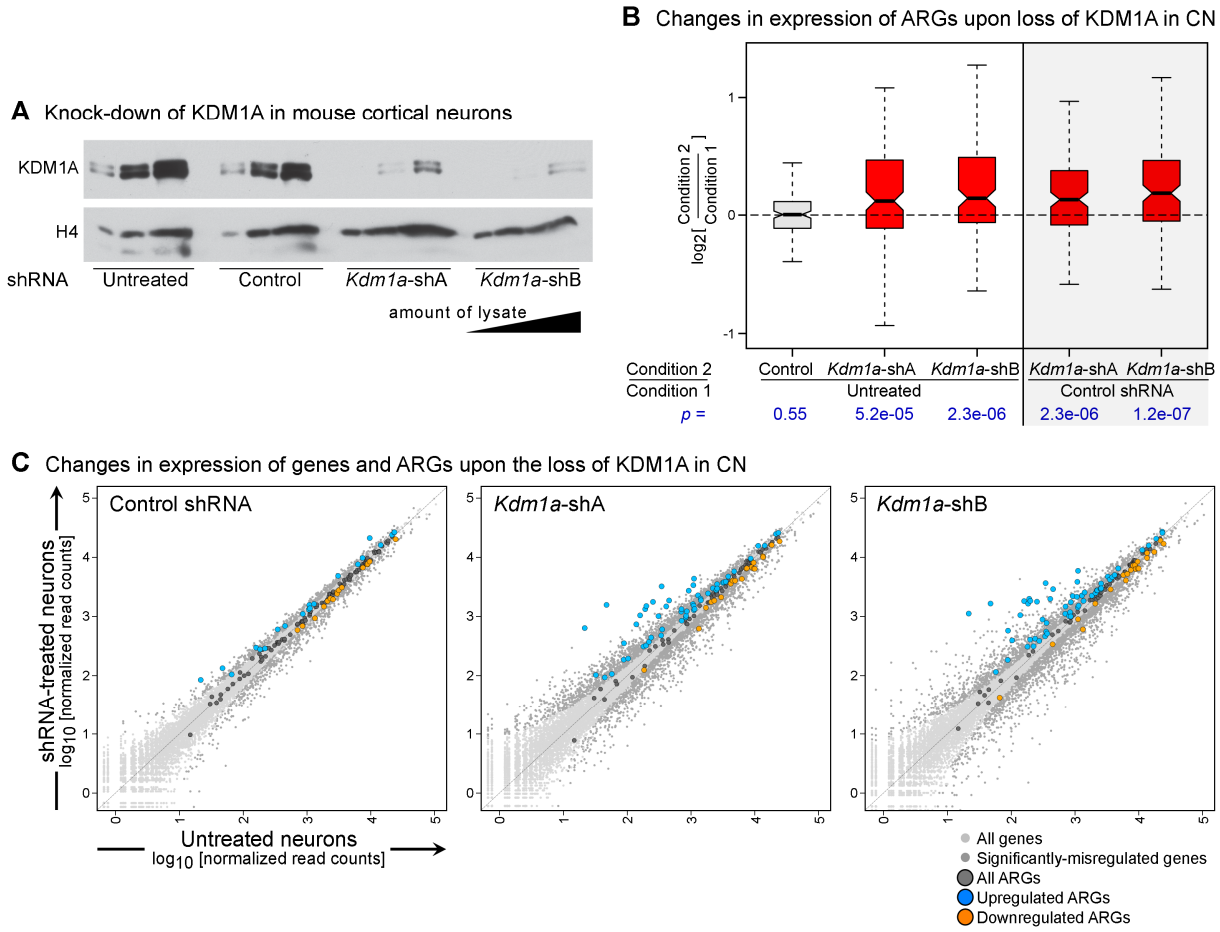

Supplemental Figure S14. Loss of KDM1A in mouse cortical neurons results in upregulation of activity-regulated genes. (**A**) Western blot analysis to confirm the knockdown (KD) of KDM1A in mouse cortical neurons (CN) at DIV 11, after 4 days of lentiviral-mediated delivery of either scrambled shRNA (control) or two independent *Kdm1a* shRNAs (A and B). (**B**) A significant upregulation of ARGs is observed in CN treated with the *Kdm1a* shRNAs but not with control shRNA (left panel). Gray box: Control shRNA vs. untreated neurons. Red boxes: *Kdm1a* shRNAs vs. untreated neurons or control shRNA. Results from the two independent *Kdm1a* shRNAs (A and B) are shown. *P*-values (*p*) from Wilcoxon signed-rank tests are denoted in blue beneath each panel. (**C**) Scatter plots of the expression levels of either all genes (smaller gray circles) or ARGs (larger circles) in shRNA-treated CN (Y-axis) and untreated CN (X-axis). Significantly-misregulated ($q < 0.05$, DESeq) genes are indicated in small dark gray circles. Significantly-upregulated and -downregulated ARGs are indicated in blue and orange, respectively.

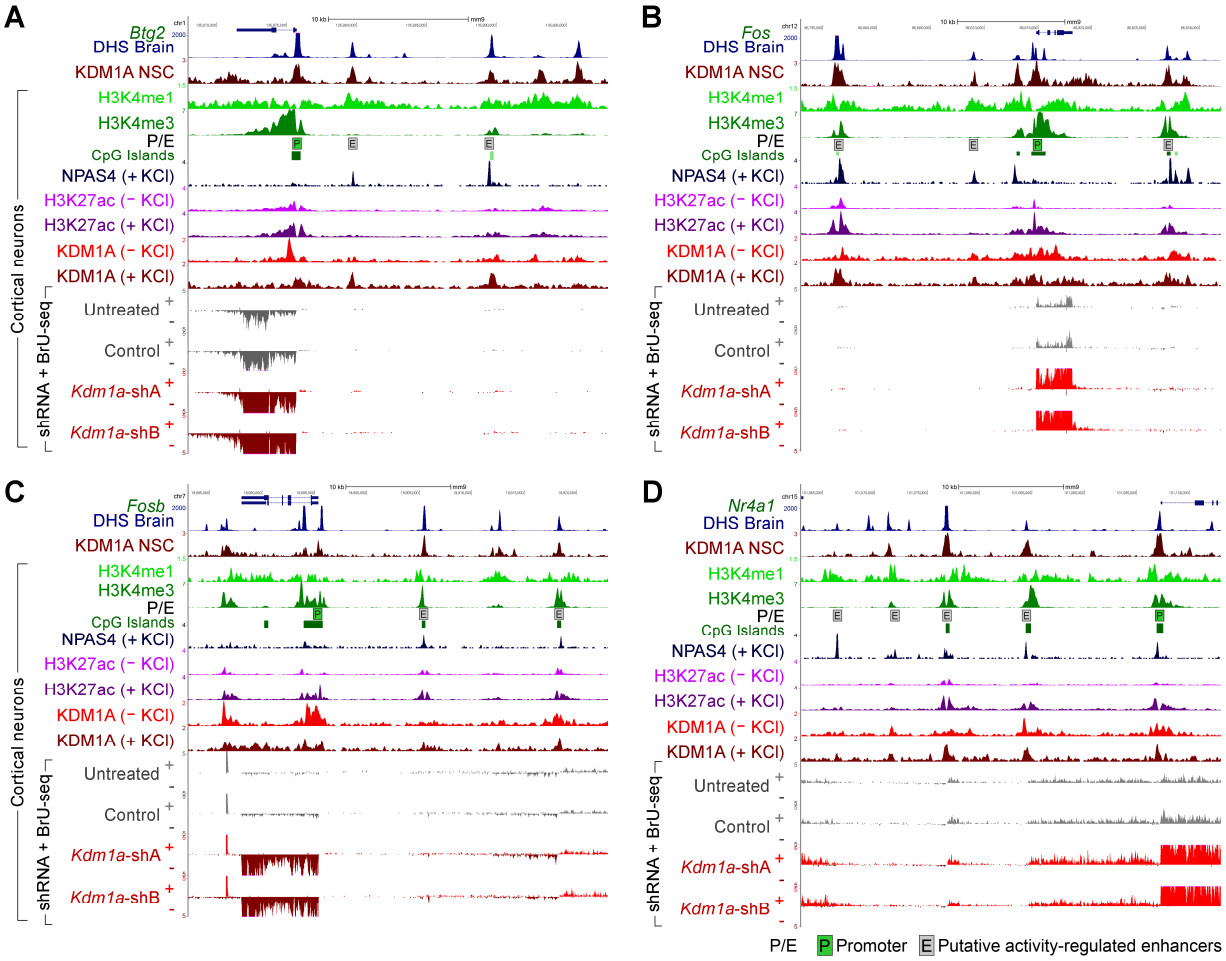

Supplemental Figure S15. Regulation of activity-regulated genes and enhancers by KDM1A in cortical neurons and their aberrant activation upon the loss of KDM1A. UCSC genome browser shots of four activity-regulated genes, *Btg2* (**A**), *Fos* (**B**), *Fosb* (**C**) and *Nr4a1* (**D**), and the nearby activity-regulated enhancers. The activity-regulated enhancers show NPAS4 binding and increases in KDM1A and H3K27ac levels after treatment with KCl (Kim et al. 2010; Malik et al. 2014). Depletion of KDM1A in cortical neurons resulted in increases in levels of both ARG mRNAs and eRNAs at some of the activity-regulated enhancers. Representative genes were selected based on the activity-dependent binding of NPAS4 within ± 50 kb of the gene. Some of the ARG enhancers overlap the CpG islands and show high H3K4me3, representing the highly-active class of enhancers (Bell and Vertino 2017).

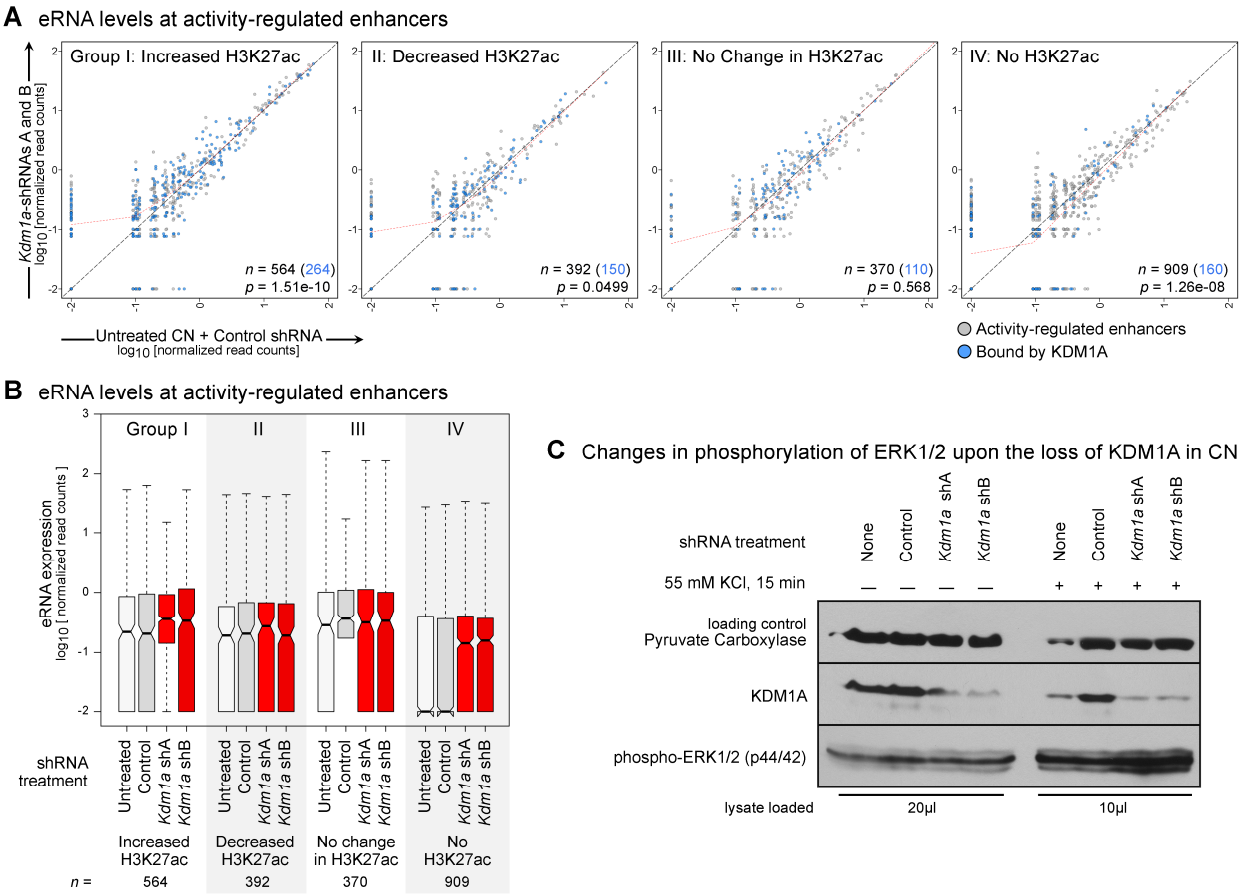

Supplemental Figure S16. Loss of KDM1A in mouse cortical neurons results in upregulation of eRNAs at activity-regulated enhancers. (**A**) Scatter plots of eRNA levels at enhancers that were divided into four groups based on the neuronal activity-induced changes in H3K27ac levels in response to KCl-mediated membrane depolarization (Malik et al. 2014). Means of normalized read counts from *Kdm1a* shRNA-treated and control shRNA-treated neurons are plotted on the Y- and X-axes, respectively. *P*-values (*p*) from Wilcoxon signed-rank tests and the total number of ARG enhancers (*n*) in each group are shown inside each panel. The numbers of KDM1A-bound enhancers are indicated in blue in parenthesis. LOWESS curve for each group is shown in red. Two groups, enhancers that gain H3K27ac upon KCl treatment and that lack H3K27ac either before or after KCl treatment, were significantly upregulated upon KDM1A knockdown. (**B**) Three groups of activity-regulated enhancers, except for the "no change in H3K27ac" group, show a trend of increased eRNA levels in *Kdm1a*-KD neurons (red boxes) compared to either untreated or control neurons (gray boxes). Results from the two independent *Kdm1a* shRNAs (A and B) are shown. Y-axis indicates the mean normalized read counts. (**C**) Western blot analysis to measure the phosphorylation levels of ERK1/2 in *Kdm1a*-KD neurons. While neuronal depolarization with 55 mM KCl results in an increase in ERK phosphorylation, shRNA-mediated depletion of KDM1A did not result in a noticeable difference in ERK phosphorylation levels compared to the control shRNA.

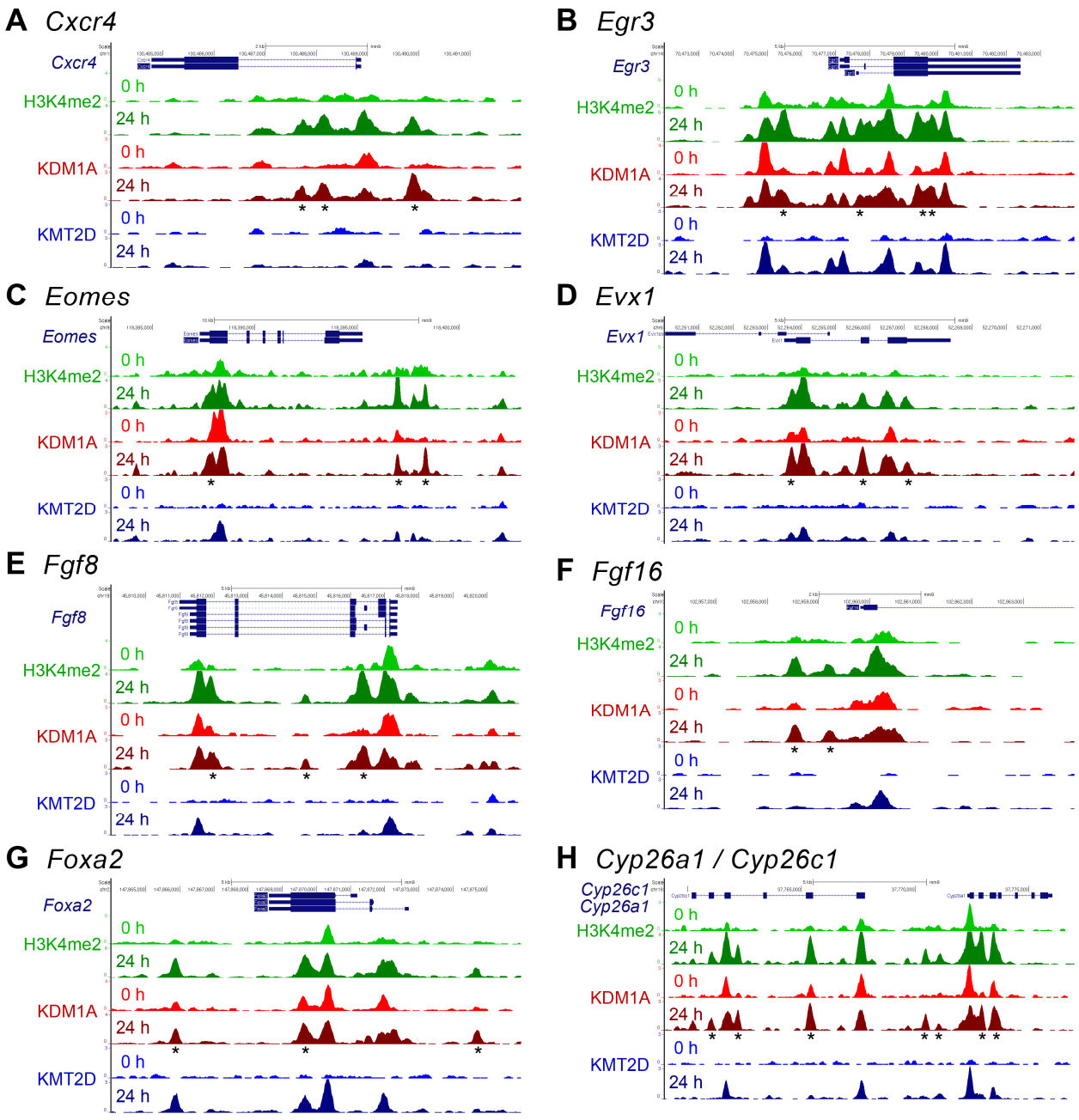

Supplemental Figure S17. Changes in H3K4me2, KDM1A, and KMT2D upon differentiation of mESCs to EpiLCs for 24 h with Activin A and FGF2. UCSC genome browser shots of eight of the induced genes (**A-H**) and the nearby enhancers. ChIP-seq signals were normalized to per million sequenced reads. Changes in H3K4me2 upon the differentiation, at promoters of the induced genes and the nearby enhancers, are accompanied with similar changes in KDM1A and KMT2D. The enhancers with visibly induced H3K4me2 and KDM1A peaks are marked by asterisks.

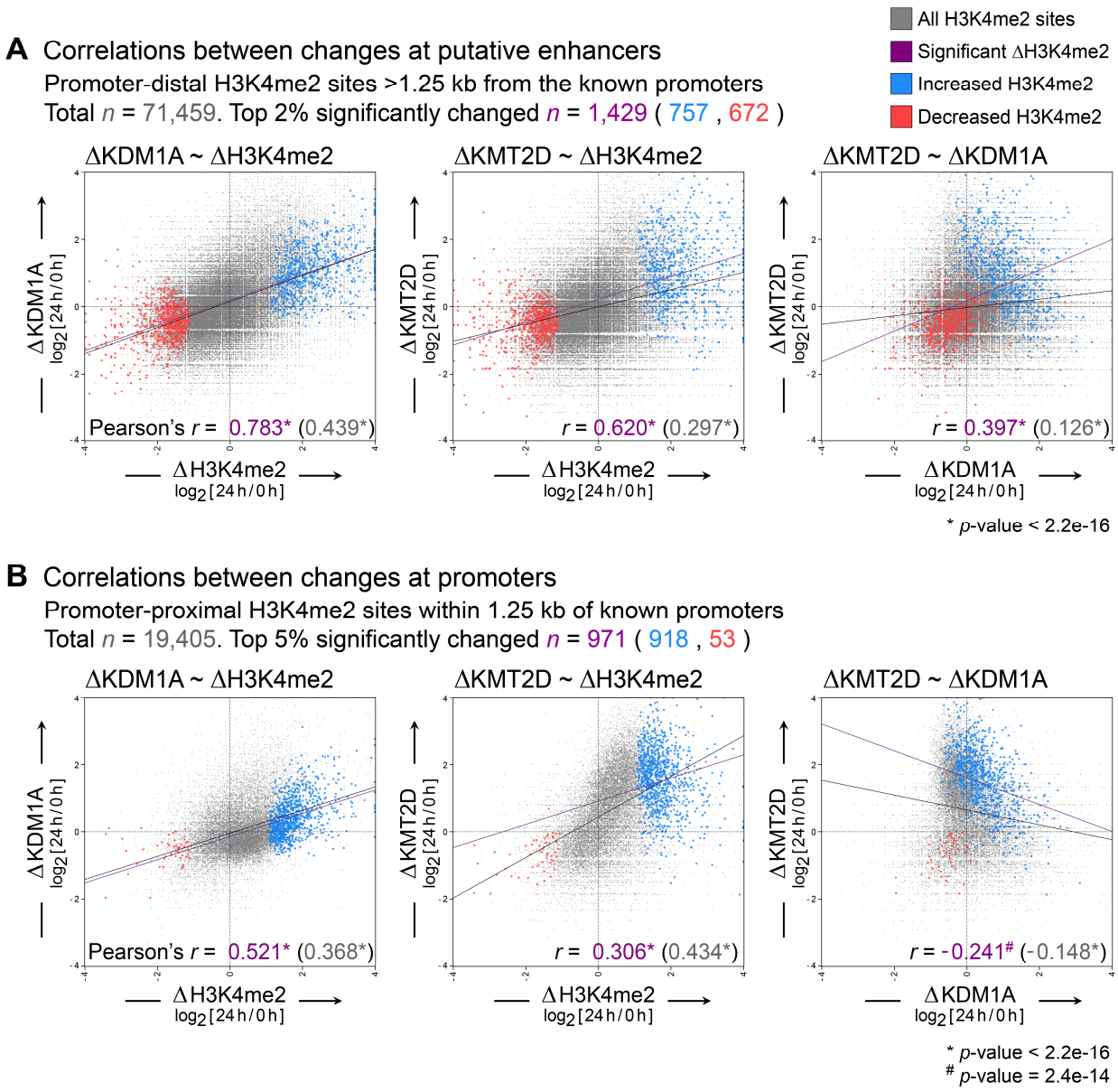

Supplemental Figure S18. Relationships between changes in H3K4me2, KDM1A, and KMT2D upon differentiation of mESCs to EpiLCs at putative enhancers and promoters. (**A**) Pearson's correlations (*r*) between changes (24 h vs. 0 h) in H3K4me2 (ΔH3K4me2), KDM1A (ΔKDM1A), and KMT2D (ΔKMT2D) at putative enhancers. At enhancers, ΔKDM1A and ΔKDMT2D show a strong and a moderately strong correlation with ΔH3K4me2, respectively. ΔKDM1A and ΔKDMT2D are also correlated positively at enhancers. 757 and 672 enhancers among the top 2% changed putative enhancers are shown in blue and red. Gray and purple lines, respectively, indicate the fitted linear models for all and top 2% changed putative enhancers. (**B**) Correlations between the changes at promoters. ΔKDM1A and ΔKDMT2D show positive but weaker correlations with ΔH3K4me2 at promoters compared to the putative enhancers. In contrast to enhancers, ΔKDM1A and ΔKDMT2D at promoters show a weak negative linear relationship. H3K4me2 ChIP-seq coverage at the 71,459 putative enhancers and 19,405 promoters was normalized using DESeq and the top 2% of enhancers and top 5% promoters with the most significant changes in H3K4me2 are shown in purple. Sites with increased and decreased H3K4me2 are shown in blue and red, respectively.

Supplemental Methods

Cultures of mES cells

Kdm1a-WT and *Kdm1a*-GT mESCs have been described previously (Macfarlan et al. 2011). Tissue culture dishes were coated with 0.1% gelatin (Sigma-Aldrich) for 30 min at 37 °C. The mESCs were cultured on the pre-coated dishes in high-glucose DMEM containing 15% ES-qualified fetal bovine serum (FBS, Chemicon), 2 mM glutamine, 1 × penicillin-streptomycin, 1 × non-essential amino acids, 10 mM HEPES, 143 μM β-mercaptoethanol (Sigma-Aldrich) and 1,000 U ml^{-1} of Leukemia Inhibitory Factor (LIF, Chemicon) in a humidified incubator at 37 °C with 5% CO_2. For differentiating mESCs to EpiLCs, the mESCs were plated on dishes coated with 15 μg/ml fibronectin (F1141, Sigma-Aldrich) and the medium was replaced with Neurobasal medium with 1 × N-2 and B-27 supplements, 20 ng/ml Activin A (338-AC, R&D Systems), and 10 ng/ml FGF2 (233-FB, R&D Systems).

For mESCs, medium was replaced every day, and Trypsin-EDTA was used for dissociation during passaging. All reagents for cell culture were from Life Technologies/Thermo Fisher unless mentioned otherwise.

Derivation of *Kdm5c*-KO mESCs

Kdm5c-KO mESCs were derived from the previously described mESCs that carry the floxed *Kdm5c* allele (Iwase et al. 2016). To delete the floxed exons 11 and 12, we transfected the *Kdm5c*-flox mESCs with pBS185 carrying a CMV promoter-driven Cre recombinase expression cassette. The resulting colonies were then isolated and genotyped to screen for the *Kdm5c*-KO mESCs as described previously (Iwase et al. 2016). The targeted *Kdm5c* allele was designed to lose the two exons as well as *Neo* by the Cre treatment (Iwase et al. 2016). Control mESCs for the *Kdm5c*-KO were obtained by transfecting the *Kdm5c*-flox mESCs with pCAG-Flpe-myc to delete the *Neo*. pBS185 and pCAG-Flpe-myc were generous gifts from Dr. Takashi Sado (National Institute of Genetics, Japan) and Dr. Constance Cepko (Harvard Medical School).

Western blot analysis

Western blot analyses were carried out using standard protocols. mESCs or cortical neurons were lysed in Laemmli sample buffer, sonicated, and subjected to SDS-PAGE. We used the following antibodies: anti-H3K4me1 (ab8895, Abcam), anti-H3K4me2 (ab7766, Abcam), anti-H3K4me3 (ab8580, Abcam), anti-H3K27ac (39135, Active Motif), anti-KDM1A (ab17721, Abcam), anti-KDM5C (Iwase et al. 2016), and anti-phospho-ERK1/2 (4370, Cell Signaling Technology).

cDNA complementation and eRNA measurement

Human *KDM1A*-WT and *KDM1A*^{K661A} cDNAs were cloned into pHAGE-Strep-Puro plasmid and lentiviruses were packaged as described previously (Garay et al. 2020). *Kdm1a*$^{flox/flox}$: Cre-ER^{T} mESCs

(Wang et al. 2007) were infected with the lentiviruses carrying either *KDM1A*-WT, *KDM1A*^{K661A}, or no cDNA and selected with 1 μg/ml puromycin for 2 days. KDM1A was depleted by treating the selected cells with either 1 μM of 4-Hydroxytamoxifen (H7904, Sigma-Aldrich) or DMSO for 3 days. Total RNAs from the mESCs were isolated using Trizol following the manufacturer's instructions. Expression levels of eRNAs were analyzed by RT-qPCR. Sequences of the oligonucleotides used are available in Supplemental Table S4. Threshold cycles of eRNAs (C_t) were normalized to those of *Tbp* mRNA, and differences in the threshold cycles (ΔC_ts) were used in the two-tailed unpaired Students' *t*-tests.

***Kdm1a* knockdown in mouse cortical neurons**

Brains from E16.5 mouse (CD1 IGS, Charles River Laboratories) were dissected, and the primary cultures of cortical neurons were carried out as described previously (Iwase et al. 2016). pLKO.1 plasmids carrying either the scrambled shRNA (SHC202, Sigma-Aldrich) or one of the two *Kdm1a*-shRNAs (A: TRCN0000071375 and B: TRCN0000071376, Sigma-Aldrich, Moffat et al. 2006) were transfected into 293T cells along with the two packaging plasmids pMD2.G and psPAX2 (Addgene) using TransIT-293 transfection reagent (Mirus) for 48 h. Viruses were concentrated using Lenti-X concentrator (Clontech) and resuspended in Neurobasal media. Viral titers were measured by the transduction of neuronal cells and assessing the survival rate at 0.2 μg/ml of puromycin for 2 days. The minimum viral concentration of each shRNA that resulted in the least cell death under this selection was used for the experimental samples. However, the experimental cultures were not treated with puromycin. CN cultures were transduced on DIV 7 and harvested on DIV 11 after 32 min of 5-bromouridine labeling.

ChIP-seq

Antibodies used for chromatin immunoprecipitation (ChIP) included anti-H3K4me1 (ab8895, Abcam and 07-436, EMD Millipore), anti-H3K4me2 (05-790, EMD Millipore), anti-H3K4me3 (04-745, EMD Millipore), anti-H3K27ac (39135, Active Motif), anti-HDAC1 (A300-713A, Bethyl Laboratories and sc-6298, Santa Cruz Biotechnology), anti-KDM1A (ab17721, Abcam), anti-KMT2D (701869, Invitrogen), and anti-KDM5C (Iwase et al. 2016). KDM5C ChIP-seq experiments were performed as described previously (Iwase et al. 2016).

ChIP-seq experiments in *Kdm1a*-WT and *Kdm1a*-GT mESCs were performed as described previously (Li et al. 2003) with minor modifications. Upon reaching confluence, the culture medium was aspirated off, and 35 ml of high-glucose DMEM containing 1% formaldehyde (Sigma-Aldrich) was added to 15 cm plates. Cells were cross-linked for 30 min in a 37 °C incubator followed by the addition of glycine to a final concentration of 125 mM. After mixing and a brief incubation with glycine, the cells were washed three times with ice-cold PBS, scraped, collected by centrifugation, and frozen at -80 °C. Approximately 100 million cells were lysed by resuspension in 40 ml of ice-cold lysis buffer CL1 (100 mM Tris pH 8, 5 mM EDTA, 1% Triton X-100 and 1% sodium deoxycholate (DOC)) containing 2 × Complete™ protease inhibitor cocktail (PIC, Roche) followed by rotation at room temperature for 30 min. Nuclei were collected

by centrifugation and resuspended in 40ml of ice-cold lysis buffer CL2 (50 mM Tris pH 8, 5 mM EDTA, 1% IGEPAL CA-630, 300 mM NaCl, 10% glycerol, and 1 × PIC) followed by rotation at room temperature for 30 min. Nuclei were again collected by centrifugation and resuspended in 40ml of ice-cold lysis buffer CL3 (50 mM Tris pH 8, 5 mM EDTA, 1% Triton X-100 and 1 × PIC). After rotation at 4 °C for 30 min, nuclei were collected by centrifugation. 4 ml of sonication buffer (50 mM Tris pH 8, 2.5% Triton X-100, 0.25% DOC and 2 × PIC) was added, and nuclei were sonicated on ice with a micro-tip of Branson Sonifier S-450 for 30 cycles (20 sec ON and 40 sec OFF). Chromatin was centrifuged at 4,000 g for 15 min at 4 °C to remove the debris. 1.6 ml of 5 × PIC, 1.6 ml 50% glycerol was added, and the total volume was adjusted to 8 ml with TE (10 mM Tris pH 8 and 1 mM EDTA). After rotation at 4 °C for 5 min, chromatin was flash-frozen on dry ice and stored at -80 °C.

10 µg antibody was immobilized on 35 µl of pre-washed Dynabeads Protein G (Thermo Fisher) in binding buffer (1 × PBS, 1 mM EDTA, and 0.25% IGEPAL CA-630 containing 5 mg/ml BSA (Sigma-Aldrich)) with overnight rotation at 4 °C. Bead-antibody conjugates were washed three times with 1 ml ice-cold binding buffer. 125 µl of binding buffer, 125 µl of 10 × PIC, and 1000 µl of sonicated chromatin were added to the beads, and the tubes were rotated at 4 °C. After overnight incubation, immunoprecipitates were washed three times with 1 ml of low-stringency buffer (50 mM Hepes pH 7.8, 1 mM EDTA, 1% IGEPAL CA-630, 0.2% DOC, 150 mM NaCl and 1 × PIC, 4 °C) followed by three washes with high-stringency buffer (50 mM Hepes pH 7.8, 1 mM EDTA, 500 mM LiCl, 1% IGEPAL CA-630, 0.7% DOC and 1 × PIC, 4 °C) and two washes with buffer LW (50 mM Tris pH 8, 5 mM EDTA and 0.25% IGEPAL CA-630, 4 °C). 150 µl of elution buffer (50 mM Tris pH 8, 5 mM EDTA and 1% SDS) was added, and immunoprecipitates were eluted from the beads by shaking at 65 °C using an Eppendorf Thermomixer for 20 min. ChIP samples and 25 µl of input chromatin were reverse cross-linked by overnight incubation at 65 °C. 150 µl of Protease solution (5 × TE pH 8 containing 7 µl of Proteinase K (New England Biolabs (NEB)) and 80 µg of glycogen (AM9510, Thermo Fisher)) was added, and samples were incubated at 42 °C for 4 h. Proteinase K was inactivated by phenol-chloroform extraction, and DNA was precipitated with ethanol. Pellets were resuspended in 100 µl of RNase solution (5 × TE pH 8 containing 20 µg of RNase A (EN0531, Thermo Fisher)) and incubated at 42 °C for 2 h. Samples were column purified (MinElute PCR purification kit, Qiagen) and eluted in warm 75 µl of IDTE pH 8 (10 mM Tris pH 8, 0.1 mM EDTA, Integrated DNA Technologies (IDT)). 50 ng of input DNA was used for library preparation.

To generate the sequencing libraries, 25 µl of phosphorylation mix, containing 10 µl of 10 × T4 DNA Ligase buffer and 2 µl of T4 Polynucleotide Kinase, was added, and samples were incubated at 37 °C for 1. 30 µl of Blunting mix, containing 6.5 µl of 10 × NEBuffer 3, 1.3 µl of 10 mg/ml BSA, 13 µl of 10mM dNTPs each and 0.3 µl of T4 DNA polymerase, was added and samples were incubated at 12 °C for 30 min. Samples were extracted with phenol-chloroform, column purified, and resolved in 75 µl of IDTE pH 8. Next, 3' dA-tailing of DNA was performed by adding 25 µl of dA-tailing mix containing 10 µl of 10 × NEBNext dA-tailing Buffer and 2 µl of Klenow Fragment (3′→5′ exo-). Samples were column purified

and eluted in 40 µl of IDTE pH 8. 10 µM adaptor mix (1 µl of 10 × NEBuffer 3.1, 1 µl of 10mg/ml BSA and 1 µl each of 10 µM CHIPADP_F (5'-CTCTTTCCCTACACGACGCTCTTCCGATC*T-3') and 10 µM CHIPADP_R (5' -/5Phos/GATCGGAAGAGCACACGTCTGAAC*TCC/3C6/-3') was added. /5Phos/ indicates modification with a 5' phosphate moiety and * indicates a phosphorothioate linkage. Ligation of adaptors to dA-tailed DNA samples was initiated by the addition of 102 µl of Ligase mix containing 100 µl of 2 × Quick Ligation reaction buffer and 2 µl of Quick T4 DNA ligase followed by incubation at 20 °C for 4 h. Samples were purified using MinElute Reaction Cleanup Kit (Qiagen) and size-selected using 2 volumes of RNAClean XP beads (Beckman Coulter). Size selected libraries were column purified and amplified for 18 cycles of PCR using CHIP_UniF: 5'-AATGATACGGCGACCACCGAGATCTACACTCTTTCCCTACACGACGCTCTTCCGATC*T-3' and reverse primer CHIP_R_x: 5′-CAAGCAGAAGACGGCATACGAGAT××××××GTGACTGGAGTTCAGACGTGTGCTCTTCCGATC*T-3', where ×××××× indicates the 6-nucleotide sequence for Illumina indexing oligonucleotide *x* for multiplexing. ChIP libraries from WT and mutant cell lines were pooled, and 280 – 600 bp fragments were gel-purified for sequencing. All enzymes and buffers used for molecular biology were from NEB. All oligonucleotides in this study were procured from IDT unless mentioned otherwise.

For the ChIP-seq in mESCs and EpiLCs, cells were cross-linked with 1% formaldehyde for 30 min at room temperature followed by quenching with 125 mM glycine. The cells were washed three times with PBS containing 50 mM Tris pH 7.5 and 1 mM EDTA, collected by centrifugation, and stored at -80 ºC. The cells were resuspended in 50 µl of 1 × micrococcal nuclease (MNase) reaction buffer (NEB) containing 0.1% each of Triton X-100 and DOC. 2 µl MNase (M0247, NEB) in 30 µl of 1 × MNase reaction buffer was added and the chromatins were digested for 30 min at 25 °C. The reactions were stopped with 5 µl of 100 mM EDTA followed by centrifugation at 5,000 rpm for 5 min at 4 °C to collect the nuclei. The nuclei were resuspended in 600 µl of ChIP dilution buffer containing 50 mM Tris pH 8, 75 mM NaCl, 5 mM EDTA, 1% Triton X-100, 1% DOC, 0.2 mg/ml BSA (B9000S, NEB), and 1 × PIC. Nuclei were then sonicated with QSonica Q800R at 70% amplitude for around 50 cycles (15 sec ON and 20 sec OFF) at 4 °C. Sheared cross-linked chromatin from 0.25 million *Drosophila* S2 cells was added to each chromatin sample. Equal portions of chromatins from all time points were pooled together and saved as the input. For KDM1A and KMT2D ChIPs, we also included an internal ChIP control by adding 1.6 µg of an in-house polyclonal rabbit antibody against H2Av, the fly-specific histone variant. For each ChIP, 5 µg of antibody against either KDM1A, KMT2D, or H3K4me2 was added to a chromatin sample from about 4 million cells and the reaction was rotated overnight at 4 °C. Mixtures of 25 µl Dynabeads Protein A (10002D, Invitrogen) and 25 µl Protein G (LSKMAGG10, Millipore) were washed and rotated overnight with 0.2 mg/ml BSA at 4°C. Next day, the beads were added to each ChIP reaction followed by incubation at 4 ºC for 1 h. The conjugates were washed three times with 1 ml of low-stringency buffer followed by three washes with high-stringency buffer and two washes with buffer LW. 200 µl of elution buffer (25 mM Tris pH 8, 2.5 mM EDTA, 200 mM NaCl, and 1% SDS) was added and mixed by vortexing. The

immunoprecipitates were eluted from the beads by shaking at 65 °C using an Eppendorf Thermomixer at 1,000 rpm for 2 h. Samples were treated with 140 µg Proteinase K at 65 °C for 1 h followed by treatment with 30 µg RNAse A at 37 °C for 1 h. DNA was purified through phenol-chloroform extraction, ethanol precipitation, and in-house solid phase reverse immobilization (SPRI) beads. The sequencing libraries were prepared using NEBNext Ultra II DNA Library Prep Kit for Illumina (NEB).

Total-RNA and nuclear-RNA sequencing libraries

Total-RNA sequencing libraries have been described in detail previously (Agarwal et al. 2015). Briefly, cells were lysed in TRIzol (Thermo Fisher), and RNA was isolated using RNeasy Mini Kit (Qiagen). Ribosomal RNA was depleted from total RNA using the Ribominus Eukaryote Kit for RNA-seq (Thermo Fisher). Libraries were prepared using Direct Ligation of Adapters to First-strand cDNA (DLAF) as described previously (Agarwal et al. 2015).

For isolation of nuclear RNA, mESCs were grown on 10 cm tissue culture dishes. Nuclei were isolated as described previously (Wang et al. 2011) with minor modifications. Cells were washed once with 12 ml ice-cold PBS and once with 12 ml ice-cold Swelling buffer SB1 (20 mM Tris pH 7.5, 2 mM $CaCl_2$, and 2 mM $MgCl_2$). Cell lysis was initiated by the addition of 5 ml of ice-cold Lysis Buffer N1 (Swelling buffer with 0.5% IGEPAL CA-630, and 20 U/ml of Superase.In (Thermo Fisher)) for 5 min on ice followed by scraping and trituration. Cells were collected, and 5 ml of ice-cold Lysis Buffer N2 (Lysis Buffer N1 with 40% glycerol) was added and mixed to homogeneity. Nuclei were incubated on ice for 5 min and collected by centrifugation at 1,000 g for 10 min at 4°C. Nuclei were resuspended in 1.5 ml of ice-cold Nuclei Wash Buffer (10 mM Tris pH 7.5, 1 mM $CaCl_2$, 1 mM $MgCl_2$, 0.25% IGEPAL CA-630, 20% glycerol, and 20 U/ml of Superase.In), incubated on ice for 2 min and centrifuged at 500 g for 2 min and 1,000 g for 1 min. Nuclei were resuspended in 600 µl of TRIzol (containing 20 µg of glycogen and 5 mM EDTA) and homogenized using a Qiashredder (Qiagen). Isolation of RNA, depletion of rRNA, and preparation of sequencing libraries were identical to that for total RNA except that oligonucleotide T9VN (5′-TTTTTTTTTVN-3′) was excluded during reverse transcription.

Global run-on transcription assay

Global run-on (GRO) was modified from the methods described previously (Core et al. 2008; Wang et al. 2011). Nuclei isolation for GRO was performed similarly to that for nuclear RNA-seq. WT and *Kdm1a*-GT mESCs, grown on 15 cm tissue culture dishes, were washed once with 25 ml ice-cold PBS and once with 25 ml ice-cold Swelling buffer SB2 (20 mM Tris pH 7.5, 1 mM $CaCl_2$, 1 mM $MgCl_2$, and 0.1 mM EDTA). Cell lysis was achieved by the addition of 6 ml of ice-cold Lysis Buffer G1 (25 mM Tris pH 7.5, 2 mM $CaCl_2$, 2 mM $MgCl_2$, 0.1 mM EDTA, 0.5% IGEPAL CA-630 and 20 U/ml of Superase.In) for 5 min on ice followed by scraping and trituration. Cells were collected, and 6 ml of ice-cold Lysis Buffer G2 (Lysis Buffer G1 with 40% glycerol) was added and mixed to homogeneity. Nuclei were incubated on ice for 5 min and were collected by centrifugation at 1,000 g for 10 min at 4°C. Nuclei were resuspended in

1.5 ml of ice-cold Nuclei Wash Buffer (10 mM Tris pH 7.5, 1 mM $CaCl_2$, 1 mM $MgCl_2$, 0.05 mM EDTA, 0.25% IGEPAL CA-630, 30% glycerol, and 20 U/ml of Superase.In), incubated on ice for 2 min and centrifuged at 500 g for 2 min and 1,000 g for 1 min. Nuclei were resuspended in 900 µl of ice-cold Freezing Buffer (20 mM Tris pH 7.5, 10 mM $MgCl_2$, 0.05 mM EDTA, 0.2% IGEPAL CA-630, 30% glycerol, and 40 U/ml of Superase.In), incubated on ice for 2 min and centrifuged at 500 g for 2 min and 1,000 g for 1 min. Nuclei were resuspended in 80 µl of Nuclei Resuspension Buffer (25 mM Tris pH 7.5, 5 mM $MgCl_2$, 0.1 mM EDTA, 0.15% IGEPAL CA-630, 25% glycerol, 50 mM KCl, 0.5 mM DTT, and 40 U/ml of Superase.In). Global Run-On reaction was started by adding 80 µl of GROmix (30 mM Tris pH 8, 10 mM $MgCl_2$, 250 mM KCl, 0.05 mM EDTA, 0.3% IGEPAL CA-630, 0.5% Sarkosyl (L7414, Sigma-Aldrich), 2.5 mM DTT, 15% glycerol, 12 µM CTP, and 0.8 mM each of ATP, GTP, and Br-UTP). GROmix was mixed with a razor-cut pipette tip (~2 mm bore) to reduce damage to chromatin, and samples were incubated at 30 °C for 8 min. This included one change from the GRO performed on *Kdm5c* mESCs, where the GROmix had contained 1% Sarkosyl instead of 0.5%. For GRO of cortical neurons, approximately 10 million neurons were cultured on 10 cm dishes. After isolation (as detailed above), nuclei were resuspended in 60 µl of Nuclei Wash Buffer, and 40 µl of GROmix, containing 0.5% Sarkosyl, was added.

Preparation of GRO-seq libraries

GRO was stopped by the addition of 3 volumes of TRI Reagent BD, and samples were homogenized with a Qiashredder. RNA was isolated by phase-separation and isopropanol precipitation. RNA was fragmented in 60 µl of 0.5 × RNA Fragmentation Reagents (AM8740, Thermo Fisher) at 70 °C for 10 min. Fragmentation was stopped by adding EDTA to 10 mM, and RNA was column purified using RNeasy Plus Mini Kit (Qiagen) and eluted in 200 µl of IDTE pH 7.5. Anti-BrdU agarose beads (sc-32323 AC, Santa Cruz Biotechnology) were blocked with 1 × SSPE (Thermo Fisher) containing 0.4% Triton X-100 and 10 × Denhardt's solution (70468, Affymetrix) for 1 h at 4°C followed by three washes with the same buffer. RNA samples were denatured at 65 °C for 5 min and cooled on ice. Denatured RNAs were incubated with anti-BrdU beads in 0.5 × SSPE, containing 0.2% Triton X-100, 1 × Denhardt's solution, and 40 U/ml of Superase.In, for 1 h 30 min at 4 °C. Beads were washed once with LSWB (0.5 × SSPE , 0.2% Triton X-100, and 20 U/ml of Superase.In), once with HSWB (1 × SSPE , 0.4% Triton X-100, and 20 U/ml of Superase.In), once with LSWB, once with TET (10 mM Tris pH 7.5, 0.1 mM EDTA, 0.2% Triton X-100, and 20 U/ml of Superase.In), once with LSWB, and once with TET. 200 µl of SDS elution buffer (TE pH 7.5 containing 0.5% SDS, 240 µg Proteinase K, and 60 µg glycogen) was added to the beads, and the samples were incubated at 42 °C with intermittent mixing for 1 h.

Immunoprecipitated RNA was purified by phenol-chloroform extraction and isopropanol precipitation. RNAs were column purified and treated with 8 U of TURBO DNase (Thermo Fisher) for 2 h at 37 °C. RNAs were column purified and 3' dephosphorylated with 25 U of Antarctic Phosphatase for 1 h at 25 °C and 1 h at 37 °C. RNAs were extracted with phenol-chloroform, column purified, and resolved in 30 µl of IDTE pH 7.5. RNAs were polyadenylated by adding 20 µl of PolyA Mix (containing 3.5 µl of 10 ×

Poly(A) Polymerase Reaction Buffer, 5 µl of 10 × M-MuLV Reverse Transcriptase Reaction Buffer, 5 µl of 500 µM ATP, 7 U of *E.coli* Poly(A) Polymerase, and 40 U of RnaseOUT (Thermo Fisher)) followed by incubation at 37 °C for 2 h. Polyadenylated RNAs were column purified and reverse transcribed using 1 µM of oligonucleotide GRO_RTVN: 5' -/5Phos/GAGCGTCGTGTAGGGAAAGAGTUTTUTGACTGGAGTTCAGACGTGTGCTCTTCCGATCTTTTTTTTTTTTTTTTTTVN-3' (Ultramer®) and 4 µl of AffinityScript Reverse Transcriptase (Agilent Technologies) in a total volume of 80 µl for 1 h at 48°C. Excess of GRO_RTVN was degraded by the addition of 60 µl of Exonuclease Mix (6 µl of 10 × M-MuLV Reverse Transcriptase Reaction Buffer, 3 µl Murine RNase Inhibitor and 120 U of *E.coli* Exonuclease I) and incubation at 37 °C for 45 min. Samples were extracted with phenol-chloroform and ethanol precipitated. Next, the samples were treated with 15 U of RNase H for 2 h at 37 °C followed by treatment with 125 U of RNase-I_f at 37 °C for 2 h in total volume of 100 µl. Samples were column purified and resolved in 40 µl of Buffer EB (Qiagen).

Circular ligation was performed with 250 U CircLigase II ssDNA Ligase (Epicentre) in the presence of 1 × reaction buffer supplemented with 2.5 mM $MnCl_2$, 100 µg/ml BSA, 1 µM ATP, 0.05% Triton X-100 and 1 M betaine in a total volume of 75 µl and incubation at 60 °C for 4 h, 65 °C for 30 min and 70 °C for 15 min. 75 µl of 10 × UDG Reaction Buffer was added, and the ligase was inactivated in a thermal cycler by heating at 98 °C for 1 min and 95 °C for 1 min. 50 µl of Linearization mix, containing 46 µl 10 × UDG Reaction Buffer, 10 µg BSA and 3 U of USER Enzyme, was added, and samples were incubated at 37 °C for 4 h. After phenol-chloroform extraction and precipitation, linearized cDNAs were denatured and resolved on a 7.5% acrylamide-urea (containing 10% formamide) gel. Next, 100 – 600 bp fragments were excised and shredded by centrifugation through a 0.4 mm hole. 450 µl of Gel Elution Buffer (20 mM Tris pH 8, 1 mM EDTA, 10 mM DTT, and 0.2% Triton X-100) was added, and samples were vigorously shaken overnight at 4°C. Gel pieces were removed by filtration through a 0.2 µm centrifugal filter (Pall Biosciences). Samples were extracted with phenol-chloroform and precipitated with isopropanol. Libraries were amplified for 14 to 18 cycles of PCR with GRO_F: 5'-AATGATACGGCGACCACCGAGATCTACACTCTTTCCCTACACGACGCTC-3' and reverse primer GRO_R_x: 5′-CAAGCAGAAGACGGCATACGAGAT××××××GTGACTGGAGTTCAGACGTGTGCTCTTCC-3'. Libraries from WT and mutant cell lines were pooled, and 175 – 400 bp fragments were purified from 6% polyacrylamide gels for sequencing.

BrU-seq

Cortical neurons (11 days *in vitro*, DIV), after shRNA treatment for four days, were incubated with 2 mM 5-bromouridine (850187, Sigma-Aldrich) for 32 min at 37 °C. The medium was removed and the cells were homogenized in 800 µl of Tri Reagent BD. After phase separation and precipitation, RNA was dissolved in 75 µl of water and treated with 10 U of DNase I for 2 h. To reduce the number of steps for library preparation, we designed and developed Direct Ligation of Adaptor to 3' end of RNA (DLAR), a method suitable for preparation libraries for BrU-seq.

RNA was fragmented by adding NEBNext RNA Fragmentation Buffer to 0.5 × and heating at 80°C for 20 min. RNA was column purified and treated with 25 U of Antarctic Phosphatase at 25 °C for 1 h and 37 °C for 1 h in a total volume of 100 µl. Next, 30 µl of Phosphatase Mix containing 6 µl 10 × T4 Polynucleotide Kinase Buffer, 3 µl of T4 Polynucleotide Kinase, and 2 µl of Antarctic Phosphatase was added, and RNA were incubated at 37 °C for 2 more hours. Samples were extracted with phenol-chloroform, column purified, and resolved in 75 µl of IDTE pH 7.5. Next, 38 µl of RNA Ligase Mix, containing 6 µl of 10 × T4 Polynucleotide Kinase Buffer, 2.2 µl of 1 mM ATP, 50 U T4 RNA Ligase 1, 300 U of T4 RNA Ligase 2, truncated KQ, and 20 µl of 100 µM DLAR_3' _ADPU (5' -/5Phos/CAUAGGAAGAGCACACGTCTGAACTC/3C6/-3'), was added. After incubation for 30 min at 22 °C, 120 µl of PEG Solution, containing 108 µl of 50% PEG-8000 and 12 µl of 10 × T4 Polynucleotide Kinase Buffer was added, and samples were incubated at 18 °C for 6 h. Samples were column purified and eluted in 250 µl of IDTE pH 7.5. BrU-containing RNA species were enriched with immunoprecipitation with anti-BrdU agarose beads as described above for GRO-seq. Purified RNAs were reverse transcribed, in a total volume of 90 µl, with 0.35 µM of DLAR_RT: 5'-TGGAGTTCAGACGTGTGCTC-3', at 42 °C for 1 h 30 min, 48°C for 30 min and 55°C for 15 min. Samples were column purified and were treated with RNase A under denaturing conditions, followed by treatment with RNase I_f to degrade any polyadenylated RNA. Samples were column purified, and only LEFT splint adaptor (Agarwal et al. 2015) was ligated to the 3' ends of cDNAs as described for the RNA-seq libraries. Ligation reactions were column purified and treated with 2 U of the USER enzyme at 37 °C for 2 h. Libraries were column purified and amplified with 16 to 18 cycles of PCR with CHIP_UniF and DLAR_R_x: 5'-CAAGCAGAAGACGGCATACGAGAT××××××GTGACTGGAGTTCAGACGTGTGCTCTTCC*TAT*G-3'. Libraries from untreated and shRNA-treated neurons were pooled, and 180 – 400 bp fragments were gel-purified for sequencing.

Each experiment was done concurrently on different genotypes to minimize technical variations. Detailed protocols for the preparation of samples and sequencing libraries are available upon request.

Sequencing and alignment

Multiplexed libraries were subjected to single-end sequencing on Illumina HiSeq 2000/2500 instruments using standard oligonucleotides designed for multiplexed paired-end sequencing, except that BrU-seq indices were sequenced with DLAR_Index_Read:5'-CATAGGAAGAGCACACGTCTGAACTCCAGTCAC-3'. ChIP-seq reads were mapped to the mm9 genome using Bowtie1 (v1.1.2) (Langmead et al. 2009), allowing for up to two mismatches. Only uniquely mapping reads were analyzed further. ChIP-seq coverage along the genome was obtained by extending the reads to a total length of 200 bp using BEDTools (v2.25.0)(Quinlan and Hall 2010). RNA-seq libraries were mapped to the mm9 genome and transcriptome using TopHat2 (v2.1.0)(Kim et al. 2013) with Bowtie2 (v2.2.6)(Langmead and Salzberg 2012). For GRO-seq and BrU-seq, full-length reads were first aligned using Bowtie1 or Tophat2, respectively. Adaptor sequences were trimmed from the unmapped

reads using BBDuk utility (Bushnell 2014), and reads were remapped and merged to the reads from the initial alignment. Only uniquely mapping reads were retained for further analysis, and the libraries were normalized to the total number of non-mitochondrial and non-ribosomal reads. For the analysis of ChIP-seq libraries from mESCs and EpiLCs that were spiked-in with drosophila reads, the first 50 bases of reads were mapped to a merged index of mouse (mm9) and drosophila (dm6) genomes as above. The reads mapping to the drosophila genome were discarded after initial counting.

Analysis

FeatureCounts (Liao et al. 2014) was used for calculating the number of reads for various genomic features. Coverage calculation and intersection analyses were done using BEDTools. MACS2 (v2.1.0) (Zhang et al. 2008) was used to call ChIP-seq peaks. DESeq (v1.22.1) (Anders and Huber 2010) was used for normalization and differential gene expression analyses. MicroRNAs, snoRNAs, and 10-20 highly expressed genes were excluded from further RNA-seq analysis.

Published ChIP-seq and DHS datasets were downloaded from various online sources, aligned, and converted to normalized bigwig files. Datasets showing good enrichment (See Supplemental Table S1) were merged for further analysis. For this purpose, we ignored the strain of mESCs from which these datasets were obtained under the assumption that these cell lines should not be significantly different from the mESC lines used in this study. Secondly, we assumed that if datasets from different mESC strains were to be merged, any minor differences occurring as a result of genomic variations or culture conditions could be minimized. Hotspot (v4.1) (John et al. 2011) was used to call hotspots from the ENCODE DHS bam files (Neph et al. 2012). HOMER (Heinz et al. 2010) was used for the identification of enriched motifs at tissue-specific hotspots outside the promoter regions (TSS $\pm$ 2000 bases). For EP300, CTCF, and KDM5C, reads from multiple replicates were merged into a single bam file before calling peaks using MACS2.

For studying changes in histone modifications in mESCs upon KDM1A loss (Fig. 2), ChIP-seq signals for H3K4me2, H3K4me3, and H3K27ac were normalized using MAnorm (Shao et al. 2012) with the fraction of reads aligning within the common peaks of WT and *Kdm1a*-GT mESCs samples from each replicate. ChIP-seq coverage profiles from only one replicate, which did not require MAnorm normalization, were used for the figures.

Exogenous RNA expression was defined as the number of GRO-seq reads mapping within ±500 bases of the 199,209 EP300/DHS sites, including promoters, across the genome. Significantly changed EP300/DHS sites were called using DESeq to ascertain the differential expression of intergenic enhancers (Fig. 3), which formed a subset of these 199,209 EP300/DHS sites. DESeq normalized read counts were scaled to *fpkms*.

For the identification of target genes (Fig. 4B), we first classified the predicted enhancers according to the statistical significance of changes in eRNA expression: significant ($q < 0.05$), moderately significant ($0.05 \leq q < 0.25$), or unchanged ($q \geq 0.5$, and FC ≤ 25%). If a gene promoter showed HiCap

interactions (Sahlen et al. 2015) with more than one enhancer (within ± 2.5 kb), it was assigned to an enhancer using the following priority scheme: significant > moderately significant > rest > unchanged. For calling promoter-enhancer interactions based on genomic proximity (Supplemental Fig. S13), promoters were assigned to the closest enhancer, and interactions were limited to 50 kb from the TSS. Genes with no reads mapping to their transcripts in both WT and *Kdm1a*-GT mESCs were excluded from this analysis.

Activity-regulated genes were identified as genes showing a significant upregulation ($p < 0.05$, DESeq) in each of the two independent replicates of previously published RNA-seq datasets from untreated and KCl-treated CN (Iwase et al. 2016). eRNA signals in BrU-seq data were too low to obtain sufficiently-high statistical power for comparison. Therefore, we aggregated eRNA signals from the two control- and the two *Kdm1a*-KD experimental groups for this analysis (Fig. 6C, Supplemental Fig. S16A). Similar trends were observed without grouping the samples (Supplemental Fig. S16B).

Ontology analysis was carried out by LRpath (Sartor et al. 2009) using the RNA-seq data from WT and *Kdm1a*-GT mESCs.

To analyze the changes in H3K4me2, KMT2D, and KDM1A during the differentiation of mESCs to EpiLCs, we first identified high confidence peaks of H3K4me2 ($q < 0.05$, MACS2) at 0 h and 24 h. To identify genomic loci that may show either an increase or a decrease in H3K4me2 during the differentiation, a union of the narrow peaks (MACS2) at the two time points was created and any H3K4me2 sites occurring within 250 bases of each other were merged together using BEDTools. BEDTools coverage was used to calculate the number of ChIP-seq fragments overlapping with each of the 90,864 identified H3K4me2 loci. DESeq was used to normalize the coverages between the two time points and identify sites with significant changes in H3K4me2. The H3K4me2 sites were then segregated into either promoter-proximal (± 1.25 kb) or promoter-distal sites, resulting in 19,405 promoters and 71,459 putative enhancers, respectively. Promoters and putative enhancers were then ranked by the significance of H3K4me2 change. Top 5% (971) of promoters and top 2% (1,429) of putative enhancers were called as sites with significant changes in H3K4me2 (Supplemental Fig. S18). Differences between the normalized values of H3K4me2, KDM1A, and KMT2D were then used to calculate the Pearson's correlation coefficients (Supplemental Fig. S18).

References for Supplemental Information

Adamo A, Sese B, Boue S, Castano J, Paramonov I, Barrero MJ, Izpisua Belmonte JC. 2011. LSD1 regulates the balance between self-renewal and differentiation in human embryonic stem cells. *Nat Cell Biol* **13**: 652-659.

Agarwal S, Macfarlan TS, Sartor MA, Iwase S. 2015. Sequencing of first-strand cDNA library reveals full-length transcriptomes. *Nature communications* **6**: 6002.

Anders S, Huber W. 2010. Differential expression analysis for sequence count data. *Genome biology* **11**: R106.

Bell JSK, Vertino PM. 2017. Orphan CpG islands define a novel class of highly active enhancers. *Epigenetics* **12**: 449-464.

Bushnell B. 2014. BBMap short read aligner, and other bioinformatic tools. https://sourceforge.net/projects/bbmap/.
Core LJ, Waterfall JJ, Lis JT. 2008. Nascent RNA sequencing reveals widespread pausing and divergent initiation at human promoters. *Science* **322**: 1845-1848.
Foster CT, Dovey OM, Lezina L, Luo JL, Gant TW, Barlev N, Bradley A, Cowley SM. 2010. Lysine-specific demethylase 1 regulates the embryonic transcriptome and CoREST stability. *Mol Cell Biol* **30**: 4851-4863.
Grant CE, Bailey TL, Noble WS. 2011. FIMO: scanning for occurrences of a given motif. *Bioinformatics* **27**: 1017-1018.
Hakimi MA, Bochar DA, Chenoweth J, Lane WS, Mandel G, Shiekhattar R. 2002. A core-BRAF35 complex containing histone deacetylase mediates repression of neuronal-specific genes. *Proc Natl Acad Sci U S A* **99**: 7420-7425.
Heinz S, Benner C, Spann N, Bertolino E, Lin YC, Laslo P, Cheng JX, Murre C, Singh H, Glass CK. 2010. Simple combinations of lineage-determining transcription factors prime cis-regulatory elements required for macrophage and B cell identities. *Molecular cell* **38**: 576-589.
Iwase S, Brookes E, Agarwal S, Badeaux AI, Ito H, Vallianatos CN, Tomassy GS, Kasza T, Lin G, Thompson A et al. 2016. A Mouse Model of X-linked Intellectual Disability Associated with Impaired Removal of Histone Methylation. *Cell reports* **14**: 1000-1009.
John S, Sabo PJ, Thurman RE, Sung MH, Biddie SC, Johnson TA, Hager GL, Stamatoyannopoulos JA. 2011. Chromatin accessibility pre-determines glucocorticoid receptor binding patterns. *Nat Genet* **43**: 264-268.
Jouneau A, Ciaudo C, Sismeiro O, Brochard V, Jouneau L, Vandormael-Pournin S, Coppee JY, Zhou Q, Heard E, Antoniewski C et al. 2012. Naive and primed murine pluripotent stem cells have distinct miRNA expression profiles. *RNA* **18**: 253-264.
Kim D, Pertea G, Trapnell C, Pimentel H, Kelley R, Salzberg SL. 2013. TopHat2: accurate alignment of transcriptomes in the presence of insertions, deletions and gene fusions. *Genome Biol* **14**: R36.
Kulakovskiy IV, Vorontsov IE, Yevshin IS, Sharipov RN, Fedorova AD, Rumynskiy EI, Medvedeva YA, Magana-Mora A, Bajic VB, Papatsenko DA et al. 2018. HOCOMOCO: towards a complete collection of transcription factor binding models for human and mouse via large-scale ChIP-Seq analysis. *Nucleic acids research* **46**: D252-D259.
Langmead B, Salzberg SL. 2012. Fast gapped-read alignment with Bowtie 2. *Nat Methods* **9**: 357-359.
Langmead B, Trapnell C, Pop M, Salzberg SL. 2009. Ultrafast and memory-efficient alignment of short DNA sequences to the human genome. *Genome Biol* **10**: R25.
Laurent B, Ruitu L, Murn J, Hempel K, Ferrao R, Xiang Y, Liu S, Garcia BA, Wu H, Wu F et al. 2015. A specific LSD1/KDM1A isoform regulates neuronal differentiation through H3K9 demethylation. *Molecular cell* **57**: 957-970.
Li Z, Van Calcar S, Qu C, Cavenee WK, Zhang MQ, Ren B. 2003. A global transcriptional regulatory role for c-Myc in Burkitt's lymphoma cells. *Proc Natl Acad Sci U S A* **100**: 8164-8169.
Liao Y, Smyth GK, Shi W. 2014. featureCounts: an efficient general purpose program for assigning sequence reads to genomic features. *Bioinformatics* **30**: 923-930.
Macfarlan TS, Gifford WD, Agarwal S, Driscoll S, Lettieri K, Wang J, Andrews SE, Franco L, Rosenfeld MG, Ren B et al. 2011. Endogenous retroviruses and neighboring genes are coordinately repressed by LSD1/KDM1A. *Genes Dev* **25**: 594-607.
Maiques-Diaz A, Spencer GJ, Lynch JT, Ciceri F, Williams EL, Amaral FMR, Wiseman DH, Harris WJ, Li Y, Sahoo S et al. 2018. Enhancer Activation by Pharmacologic Displacement of LSD1 from GFI1 Induces Differentiation in Acute Myeloid Leukemia. *Cell reports* **22**: 3641-3659.
Malik AN, Vierbuchen T, Hemberg M, Rubin AA, Ling E, Couch CH, Stroud H, Spiegel I, Farh KK, Harmin DA et al. 2014. Genome-wide identification and characterization of functional neuronal activity-dependent enhancers. *Nat Neurosci* **17**: 1330-1339.
Moffat J, Grueneberg DA, Yang X, Kim SY, Kloepfer AM, Hinkle G, Piqani B, Eisenhaure TM, Luo B, Grenier JK et al. 2006. A lentiviral RNAi library for human and mouse genes applied to an arrayed viral high-content screen. *Cell* **124**: 1283-1298.
Neph S, Vierstra J, Stergachis AB, Reynolds AP, Haugen E, Vernot B, Thurman RE, John S, Sandstrom R, Johnson AK et al. 2012. An expansive human regulatory lexicon encoded in transcription factor footprints. *Nature* **489**: 83-90.

Outchkourov NS, Muino JM, Kaufmann K, van Ijcken WF, Groot Koerkamp MJ, van Leenen D, de Graaf P, Holstege FC, Grosveld FG, Timmers HT. 2013. Balancing of histone H3K4 methylation states by the Kdm5c/SMCX histone demethylase modulates promoter and enhancer function. *Cell reports* **3**: 1071-1079.

Quinlan AR, Hall IM. 2010. BEDTools: a flexible suite of utilities for comparing genomic features. *Bioinformatics* **26**: 841-842.

Respuela P, Nikolic M, Tan M, Frommolt P, Zhao Y, Wysocka J, Rada-Iglesias A. 2016. Foxd3 Promotes Exit from Naive Pluripotency through Enhancer Decommissioning and Inhibits Germline Specification. *Cell stem cell* **18**: 118-133.

Rusconi F, Grillo B, Ponzoni L, Bassani S, Toffolo E, Paganini L, Mallei A, Braida D, Passafaro M, Popoli M et al. 2016. LSD1 modulates stress-evoked transcription of immediate early genes and emotional behavior. *Proc Natl Acad Sci U S A* **113**: 3651-3656.

Sahlen P, Abdullayev I, Ramskold D, Matskova L, Rilakovic N, Lotstedt B, Albert TJ, Lundeberg J, Sandberg R. 2015. Genome-wide mapping of promoter-anchored interactions with close to single-enhancer resolution. *Genome biology* **16**: 156.

Sartor MA, Leikauf GD, Medvedovic M. 2009. LRpath: a logistic regression approach for identifying enriched biological groups in gene expression data. *Bioinformatics* **25**: 211-217.

Shao Z, Zhang Y, Yuan GC, Orkin SH, Waxman DJ. 2012. MAnorm: a robust model for quantitative comparison of ChIP-Seq data sets. *Genome Biol* **13**: R16.

Shen H, Xu W, Guo R, Rong B, Gu L, Wang Z, He C, Zheng L, Hu X, Hu Z et al. 2016. Suppression of Enhancer Overactivation by a RACK7-Histone Demethylase Complex. *Cell* **165**: 331-342.

Shi Y, Lan F, Matson C, Mulligan P, Whetstine JR, Cole PA, Casero RA. 2004. Histone demethylation mediated by the nuclear amine oxidase homolog LSD1. *Cell* **119**: 941-953.

Song Y, Dagil L, Fairall L, Robertson N, Wu M, Ragan TJ, Savva CG, Saleh A, Morone N, Kunze MBA et al. 2020. Mechanism of Crosstalk between the LSD1 Demethylase and HDAC1 Deacetylase in the CoREST Complex. *Cell reports* **30**: 2699-2711 e2698.

Vallianatos CN, Farrehi C, Friez MJ, Burmeister M, Keegan CE, Iwase S. 2018. Altered Gene-Regulatory Function of KDM5C by a Novel Mutation Associated With Autism and Intellectual Disability. *Frontiers in molecular neuroscience* **11**: 104.

Wang D, Garcia-Bassets I, Benner C, Li W, Su X, Zhou Y, Qiu J, Liu W, Kaikkonen MU, Ohgi KA et al. 2011. Reprogramming transcription by distinct classes of enhancers functionally defined by eRNA. *Nature* **474**: 390-394.

Wang J, Scully K, Zhu X, Cai L, Zhang J, Prefontaine GG, Krones A, Ohgi KA, Zhu P, Garcia-Bassets I et al. 2007. Opposing LSD1 complexes function in developmental gene activation and repression programmes. *Nature* **446**: 882-887.

Wang J, Telese F, Tan Y, Li W, Jin C, He X, Basnet H, Ma Q, Merkurjev D, Zhu X et al. 2015. LSD1n is an H4K20 demethylase regulating memory formation via transcriptional elongation control. *Nat Neurosci* **18**: 1256-1264.

Wang Y, Wu Q, Yang P, Wang C, Liu J, Ding W, Liu W, Bai Y, Yang Y, Wang H et al. 2016. LSD1 co-repressor Rcor2 orchestrates neurogenesis in the developing mouse brain. *Nature communications* **7**: 10481.

Zhang Y, Liu T, Meyer CA, Eeckhoute J, Johnson DS, Bernstein BE, Nusbaum C, Myers RM, Brown M, Li W et al. 2008. Model-based analysis of ChIP-Seq (MACS). *Genome Biol* **9**: R137.

Zibetti C, Adamo A, Binda C, Forneris F, Toffolo E, Verpelli C, Ginelli E, Mattevi A, Sala C, Battaglioli E. 2010. Alternative splicing of the histone demethylase LSD1/KDM1 contributes to the modulation of neurite morphogenesis in the mammalian nervous system. *The Journal of neuroscience : the official journal of the Society for Neuroscience* **30**: 2521-2532.